

Integrated Modeling of Typhoon Damrey's Effects on Sediment Resuspension and Transport in the North Passage of Changjiang Estuary, China

Qi Shen¹; Wenrui Huang²; and Dingman Qi³

Abstract: A typhoon is one of the major factors that often cause sediment transport and bed erosion in estuarine navigational channels. A 12.5-m deepwater navigational channel (DNC) is located in the north passage of the Changjiang Estuary. Because it acts as the entrance navigation waterway of the Changjiang River, it is important to investigate the impact of typhoons on sediment suspension and transport in the navigation channel. In this study, a previously calibrated hydrodynamic and sediment transport model [shallow-water equation model (SWEM)] was integrated with a storm wind model [weather research and forecasting (WRF)] and a wave model [simulating waves nearshore (SWAN)] to investigate the effect of Typhoon Damrey on the navigation channel in 2012. The typhoon produced a weak storm surge but significant wave heights in the Changjiang Estuary. By comparing bottom shear stress induced by current and wave, numerical modeling results indicated that the increase of sediment concentration in the navigation channel during Typhoon Damrey was mainly caused by sediment transport fluxed into the channel from shallow-water areas outside the channel, where wave-induced bottom shear stress during Typhoon Damrey caused sediment resuspension. The high sediment flux overtopping from the south dike into the channel was the important sediment source for the navigation channel. During the passage of Typhoon Damrey, there was a convergence area of sediment flux between the upstream seaward sediment transport and the lateral transport of sediment flux overtopping from the south dike at the middle-lower reach of the north passage. Near the outlet of the north passage, the near-bottom residual transport of sediment was in the upstream direction against the seaward sediment transport from the river. The convergences of sediment flux produced the high-turbidity maximum zone at the lower reach of the north passage, where in situ bathymetric surveys within the DNC before and after Typhoon Damrey showed the sediment deposition area in the channel. DOI: [10.1061/\(ASCE\)WW.1943-5460.0000453](https://doi.org/10.1061/(ASCE)WW.1943-5460.0000453). © 2018 American Society of Civil Engineers.

Author keywords: Navigation channel; Typhoon Damrey; Changjiang Estuary; Waves; Sediment transport; Erosion and deposition.

Introduction

Typhoons often cause morphological changes and sediment transport in coasts and estuaries (Huang 2017; Liu and Huang 2009; Neshaei and Ghanbarpour 2017). According to the China Marine Hazards Communique, storm surge in China accounted for 99.7% of the direct economic loss of total marine hazards in 2014 (State Oceanic Administration 2014). In estuaries, storm-induced surges coupled with tidal currents, waves, river flows, and gravitational circulations can often cause the erosion of coasts and tidal flats (Stone and Pepper 1997; Fan et al. 2006; Houser et al. 2008; Stockdon et al. 2007; Goleij et al. 2017), change in coastal sediment transport (Yang et al. 2007; Liu and Huang 2009; Fettweis et al. 2010; Biria et al.

2015), and deposition of sediment (Fumin et al. 2008; Palinkas et al. 2014; Freeman et al. 2015). The increased amount of sediment deposited in the navigational channel may also cause the blockage of waterways (Zhou and Li 2005). This is also true for the Changjiang Estuary because the original navigation waterway, which was located at the south passage of the Changjiang Estuary, was entirely obstructed when Typhoon 8310 went through in the summer of 1983 (Li et al. 2003). Nowadays, the north passage of Changjiang Estuary, where the 12.5-m deepwater navigational channel (DNC) is located, undertakes the main navigational outlet of the Changjiang River Delta. In consideration of the potential impact of the storm event, more efforts should be made to study the storm-induced sediment suspension and transport and the associated bed erosion and deposition in the north passage of the Changjiang Estuary.

The Changjiang Estuary (Fig. 1) is one of the typical braided-type estuaries, and its morphodynamic patterns from Xuliujing City to the mouth of the river can be described as "three-order bifurcations and four-outlet diversions into the sea" (Yan et al. 2011). The Changjiang Estuary is separated into the north branch and the south branch by Chongming Island. The south branch is further divided into the north channel and the south channel by Changxing Island and Hengsha Island, whereas the south channel is divided into the north passage and the south passage. The DNC, 92.2 km long and 350–400 m wide, was designed to cut through the river-mouth bar and extend landward along the north passage. The hydraulic engineering construction of the navigation channel, which aimed to enhance the discharge capacity of sediment transport within the channel, was composed of massive dredging and along-channel dykes and groins attached along the channel banks (Fig. 1). Engineering construction began in 1998,

¹Ph.D. Student, Dept. of Hydraulic Engineering, Tongji Univ., 1239 Siping Rd., Shanghai 200092, People's Republic of China; Senior Engineer, Shanghai Estuarine and Coastal Science Research Center, No. 1045 Xingsheng Rd., Shanghai 201201, People's Republic of China.

²Professor, Dept. of Civil and Environmental Engineering, Florida A&M Univ.–Florida State Univ., Tallahassee, FL 32312; Adjunct Professor, Tongji Univ., Shanghai 200092, People's Republic of China (corresponding author). Email: whuang@eng.famu.fsu.edu

³Senior Engineer, Shanghai Estuarine and Coastal Science Research Center, No. 1045 Xingsheng Rd., Shanghai 201201, People's Republic of China.

Note. This manuscript was submitted on August 1, 2017; approved on January 19, 2018; published online on July 24, 2018. Discussion period open until December 24, 2018; separate discussions must be submitted for individual papers. This paper is part of the *Journal of Waterway, Port, Coastal, and Ocean Engineering*, © ASCE, ISSN 0733-950X.

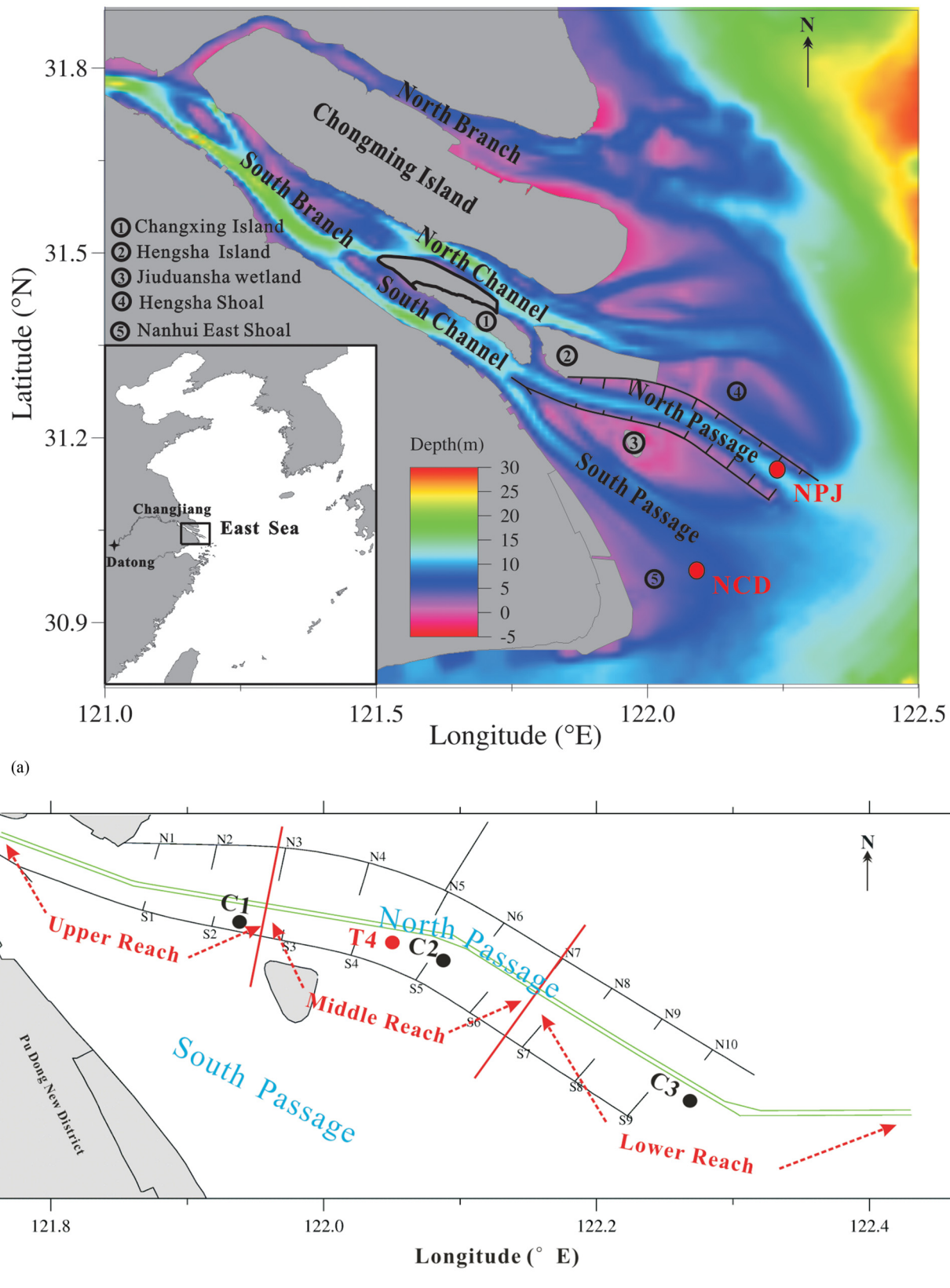


Fig. 1. (Color) Study area: (a) Changjiang Estuary; and (b) DNC at the north passage of the estuary. NCD = Nan Cao Dong Station; NPJ = Niu Pi Jiao Station. Stations C1–C3 refer to the observation stations for model calibration, and T4 refers to the observation station for model verification.

lasted for three stages, and was completed in 2010. The navigation channel is divided into three parts: the upper reach, the middle reach, and the lower reach [Fig. 1(b)].

The Changjiang Estuary is a mesotidal, partially mixed estuary with abundant water and sediment supplies. The average tidal ranges vary from 2.4 to 3.2 m, and the annual average

freshwater discharge reaches 28,527 m³/s with the peak value above 50,000 m³/s during flooding season (Chen et al. 1999). The hydrological records show that the average sediment discharge is 15 t/s or 5×10^8 t/year (Li et al. 2010). In the Changjiang Estuary, the estuarine turbidity maximum (ETM) zone is extremely large on a spatial scale, spreading over the entire mouth zone downstream from the south branch and inside the 10-m isobaths (Han and Lu 2015). The ETM is also accompanied by a shallow area (approximately 6 m) in the mouth zone, primarily the mouth bars (Pan et al. 1999; Shen et al. 1992). Due to the existence of ETM, the middle and lower reach of the DNC, which are closely adjacent to the ETM (see Fig. 1 for location), endure severe sediment backsiltation at an amount more than 70 million m³/year. According to the historical statistics of typhoon events, the average number of typhoons affecting the east sea of China is approximately 6.5, of which nearly one-third act on the Changjiang Estuary (Gu et al. 2010). The annual 2.1 typhoon events that have a direct influence on the Changjiang Estuary are believed to make a great contribution to the amount of sediment siltation in the DNC.

During the passage of a typhoon event, the surface wind, tidal current, waves, and storm surge interact in a complicated manner. Under typhoon conditions, the winds and waves interact through the waves' surface wind boundary (Chen et al. 2013). The generated wave height will modulate with the tide. An opposing tidal flow increases wave height, whereas a following tidal flow decreases wave height in a coastal region (Jia et al. 2015). Meanwhile, the storm surge influences the current velocity through the gradient of the water level and the wave radiation stress. Many researchers have conducted studies of strong typhoon effects on storm surge and dynamics (Brown et al. 2013; Palinkas et al. 2014; Yang et al. 2014, 2016), sediment transport (Jin and Ji 2005; Hu et al. 2009; Lou et al. 2016), and morphological response (Houser et al. 2008; Cañizares and Irish 2008; Dai et al. 2015). Only a few explorative studies have been conducted to discuss the storm-induced sediment transport, erosion and deposition, as well as channel siltation in the Changjiang Estuary. Based on the recorded channel siltation obtained from the Department of Channel Maintenance, Zhao et al. (2012) analyzed the storm-induced sudden sedimentation in the DNC over the last decade and claimed that the amount of sudden sedimentation caused by typhoons was between 2 million and 8 million m³/year, occupying 4–50% of the total annual amount of channel siltation. Fan et al. (2006) studied the bed level variation in response to waves through the elevation-monitoring profile measured at an interval of 1–3 days along the Donghai transect of the Nanhui mudflats and discovered that the magnitude of erosion was greater near a weak storm during spring tides than a strong storm during neap tides. Xie et al. (2017) used the terrestrial laser scanner to investigate the tidal flat morphology on a typhoon event time-scale. In addition to in situ observations, an integrated numerical model has been established to investigate the storm impacts on different coasts and estuaries (Zhao 2007; Guo et al. 2009; Liu and Huang 2009; Palinkas et al. 2014; Pan and Liu 2015; Yin et al. 2016). Ding et al. (2003) simulated a typical typhoon event and presented the storm-induced erosion and deposition along the DNC during the passage of Typhoon Jelawat without detailed discussion on the sediment transport. Li and Li (2016) combined remote sensing observations with a numerical model to study the suspended sediment concentration (SSC) variation in the East China Sea under a supertyphoon event. The results showed that spring-neap tidal effects significantly controlled the distribution and variation of SSC in the shallower coastal water (<20–30 m in depth), and the typhoon-induced resuspension was evident in the coastal waters

near the Changjiang Estuary and Hangzhou Bay. Wan et al. (2014) analyzed the mechanism and transport process of storm-induced mud fluid during the occurrence of a cold-air front at the north passage of the Changjiang Estuary with the help of field observation, hydrodynamics, and wave modeling. The study found that the behavior of the storm-induced fluid mud event mainly depended on the overall hydrodynamic regimes and the exchanges of sediment, which was released by storm-wave agitation from adjacent tidal flats. However, considering the mixed effects of currents and waves on bottom shear stress, separating wave and current effects on sediment transport during a typhoon event has not been investigated in previous studies and literatures.

In 2012, Typhoon Damrey produced strong waves in the Changjiang Estuary with a weak storm surge. It provides a good case study for investigating typhoon-induced wave effects on bottom shear stress and resulting sediment resuspension and transport. In this study, the integrated modeling study of wind, wave, and sediment transport during Typhoon Damrey was conducted to focus on the investigation of typhoon-induced wave effects on sediment resuspension in Changjiang Estuary and the sediment transport in the navigation channel by estuarine circulation. The weak storm surge during Typhoon Damrey made it easier to investigate the wave-induced changes of bottom shear stress for sediment resuspension during the typhoon.

Field Observation during Typhoon Damrey

The tenth typhoon event in 2012, named Damrey, originated from a tropical disturbance formed north of Guam on July 26, 2012 (Universal Time Code (UTC) +8, which is used in the following sections). Then, it was upgraded to a tropical storm on July 28 (Fig. 2, 1#) and became a severe tropical storm on July 31 (Fig. 2, 2#). At 8 a.m. on August 1 (Fig. 2, 3#), Damrey intensified into a tropical typhoon whose center was located at 1,080 km southeast from Shanghai and moved northwestward quickly at a speed of 30–40 km/h. At 5 a.m. on August 2 (Fig. 2, 4#), the typhoon center entered into the East China Sea with a maximum wind speed of 33 m/s and a minimum atmosphere pressure of 984 hPa. At 9 p.m. on August 2 (Fig. 2, 5#), the core of Typhoon Damrey landed near Lianyungang City, Jiangsu Province with the maximum wind speed of 35 m/s and then the wind speed was gradually decreased to normal condition until August 4 at the northeast part of the Bohai Sea (Fig. 2). After the typhoon landed, high winds appeared at the Niu Pi Jiao (NPJ) station with a maximum velocity of 14 m/s (Fig. 3).

During the impact of Typhoon Damrey, from approximately 12 a.m. on August 1 to 12 a.m. on August 5 (Fig. 3), the average significant wave height (SWH) at the Nan Cao Dong (NCD) station was 0.94 m, with a maximum value of 2.13 m occurring at 10 a.m. on August 3. The water level variation range was nearly unchanged during Typhoon Damrey, indicating very weak storm surge effect. The river flow was approximately 57,000 m³/s. Field observations showed an increase of wave height but no prominent storm surge. After the typhoon landing, the measured bottom velocity at the T4 station in the north passage [see location at Fig. 1(b)] showed a slight decrease, whereas the bottom SSC increased dramatically just after the SWH reached the maximum. The current at the T4 station was ebb-dominated. The maximum bottom ebb velocity was approximately 1 m/s, whereas the maximum flood velocity was approximately 0.8 m/s.

To investigate the bed erosion and sediment deposition during Typhoon Damrey, two boat-based topographic surveys, the pre-storm and poststorm topographic surveys, were conducted along the north passage of Changjiang Estuary on July 31, 2012 and on

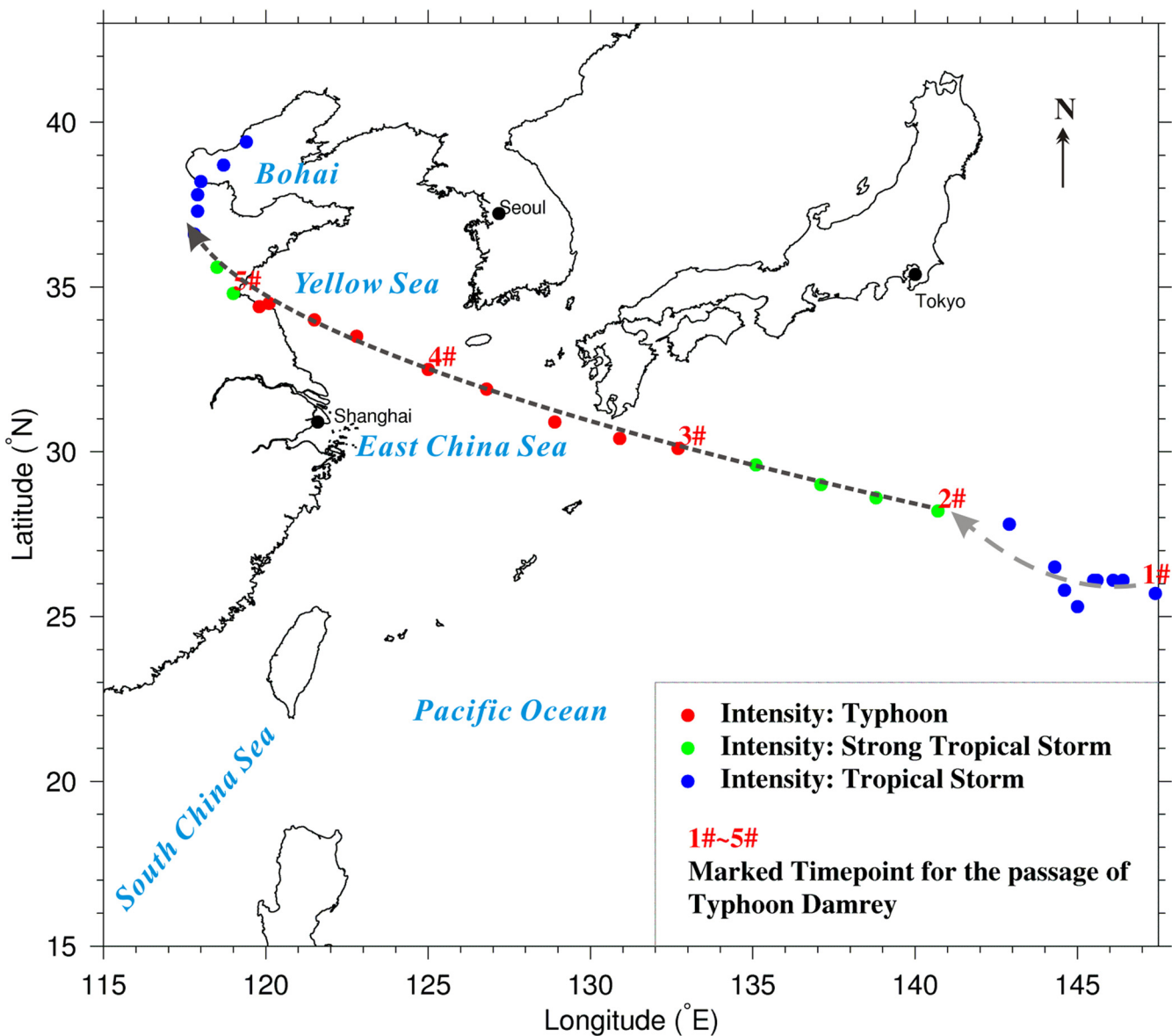


Fig. 2. (Color) Track of Typhoon Damrey (symbols refer to the different stages of typhoon intensity, and the labels 1#–5# represent the critical times as shown in Fig. 3).

August 5, 2012, respectively. In addition, during Typhoon Damrey, wave height, wind speed, and water level were automatically recorded at the gauging stations (NPJ and NCD; see Fig. 1 for location). A tripod device, which was deployed at the T4 site before the arrival of Typhoon Damrey, was used to collect the current velocity and bottom SSC during the passage of Typhoon Damrey. The tripod was equipped with one acoustic wave and current (AWAC; Nortek, Rud, Norway) with a central frequency of 1,000 kHz, one down-looking Aquadopp current profiler (ADCP; Nortek) with a central frequency of 2,000 kHz, and two optical backscattering sensors (OBS-3A, OBS-3+; D&A Instrument Company, Port Townsend, Washington) for measuring turbidity. The bottom SSC was obtained after the OBS were calibrated by in situ water samples.

Descriptions of Integrated Numerical Models

Integrated numerical modeling methods have been used by some researchers for estuarine hydrodynamic or mass transport modeling

studies by considering the atmospheric forcing, wave propagation, and tides (Jin and Ji 2005; Wang et al. 2006; Cañizares and Irish 2008; Guo et al. 2009; Brown et al. 2013; Freeman et al. 2015; Han and Kim 2015). The atmospheric forcing boundary conditions of surface wind and pressure during the passage of a typhoon event can be reproduced using the analytical wind model (Xu et al. 2005) or the regional atmospheric model (Nakamura et al. 2015). After reproducing the surface boundary of atmospheric forcing, Jin and Ji (2005) built the coupled models including the hydrodynamic model, the sediment transport model, and the third-generation wave model SWAN (simulating waves nearshore) to study the sediment process under storm conditions. Wang et al. (2006) also coupled the hydrodynamic model with the SWAN model to discuss the wave–current interaction in the Pearl River Estuary. In the wave current coupling procedure, the hydrodynamics model was run first to obtain the tidal levels and current; then, the wave model was used to obtain the distributions of wave heights and wave directions. Finally, the hydrodynamics model was run again to obtain the tidal current taking into account the interaction of waves and currents. For simulations of

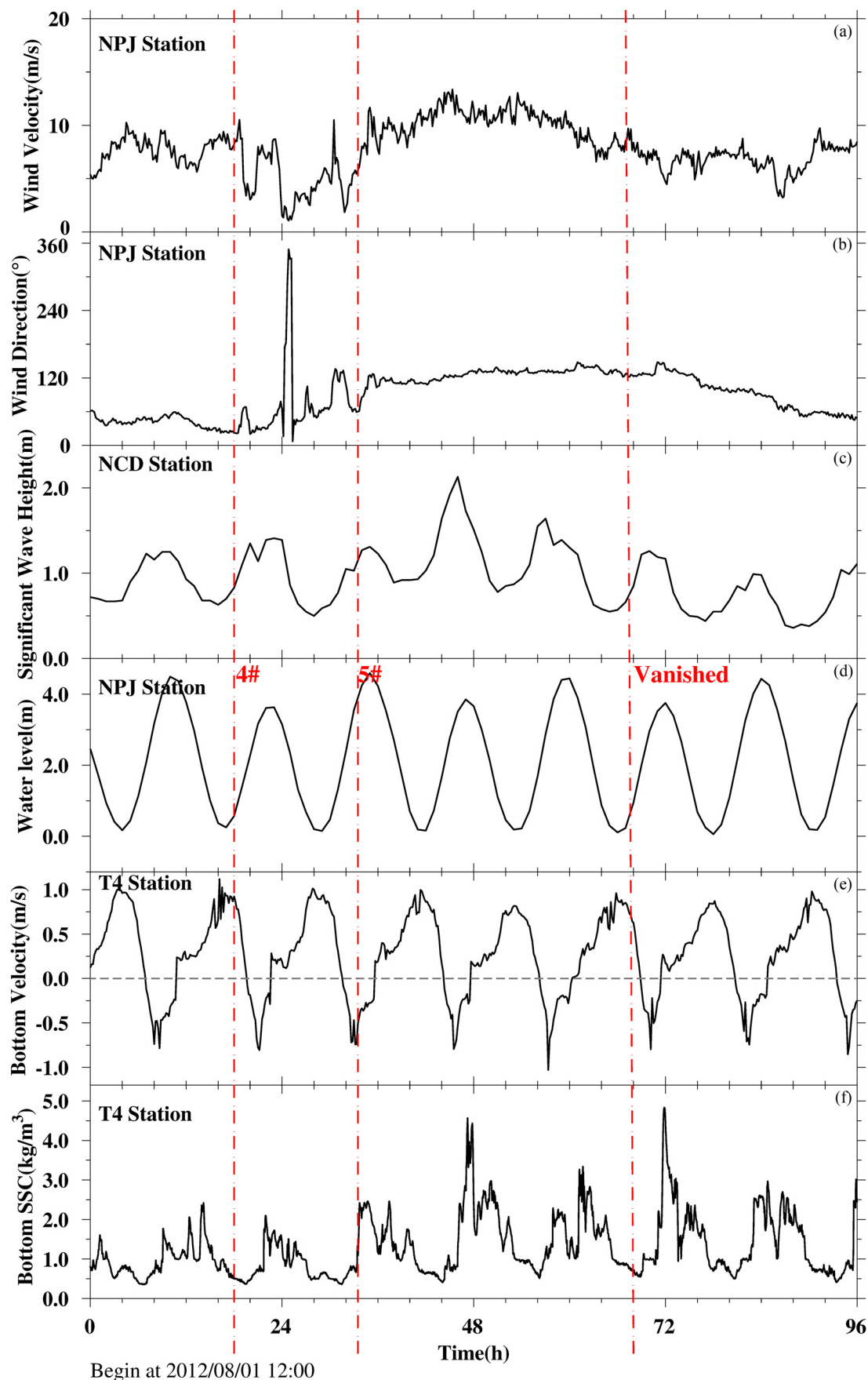


Fig. 3. (Color) Field observations: (a) wind velocity; (b) direction; (c) significant wave height (SWH); (d) water level; (e) bottom current velocity; and (f) bottom SSC during the impact of Typhoon Damrey. Note: 4# and 5# represent critical times identified in Fig. 2.

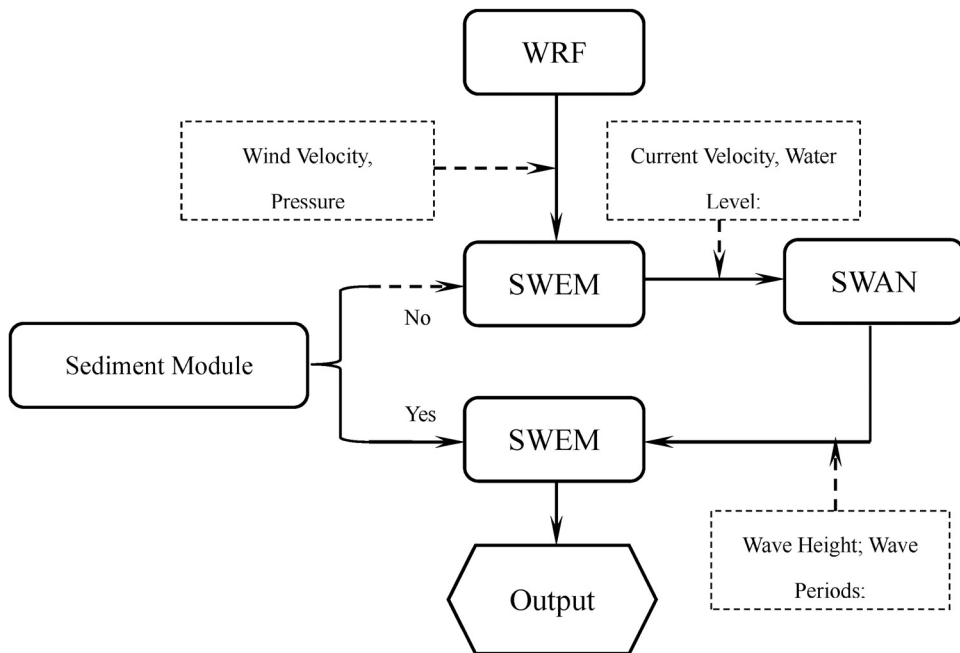


Fig. 4. Framework of integrated models including WRF, SWAN, and SWEM models.

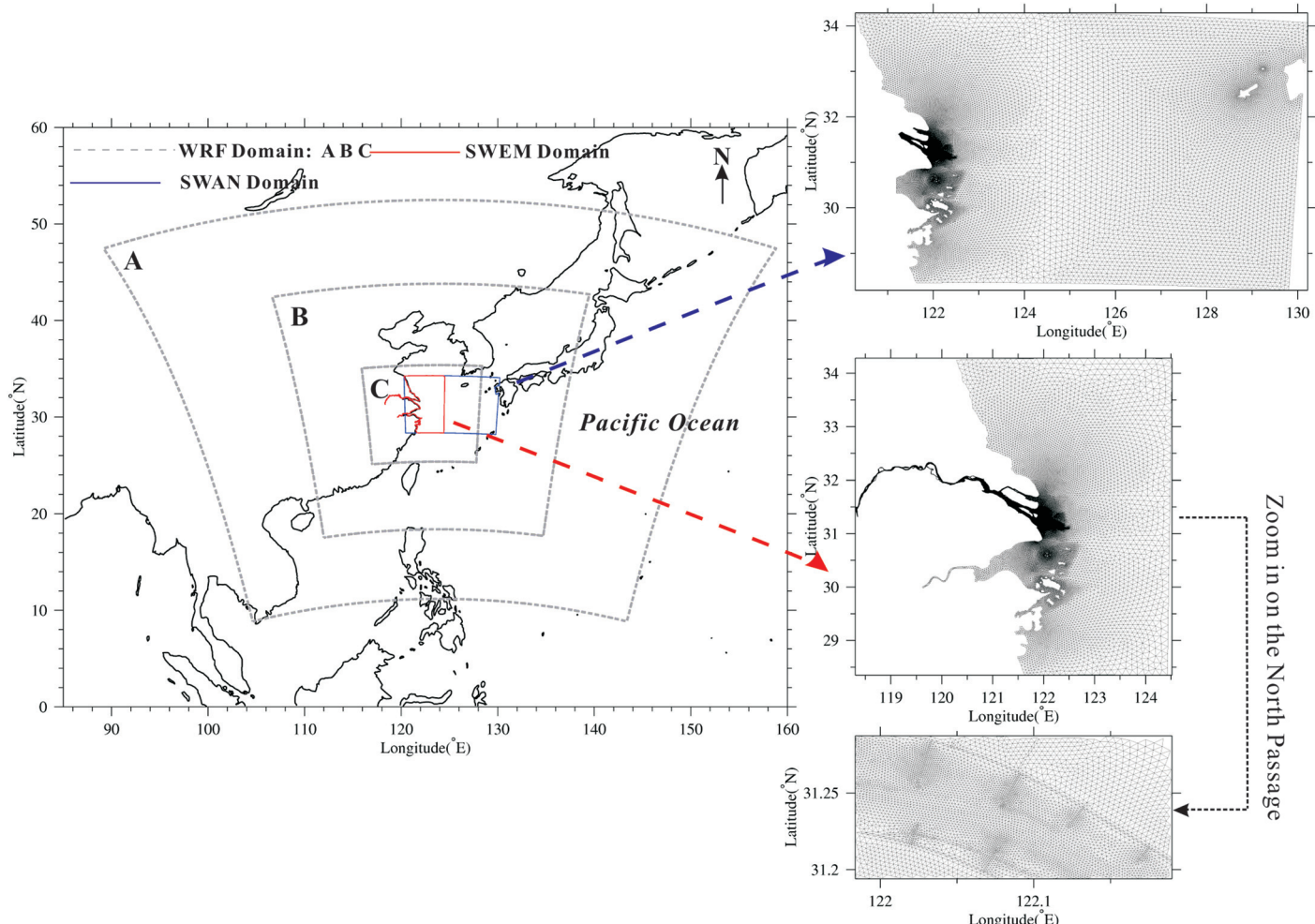


Fig. 5. (Color) Model grids of the coupled models (including the WRF model, the Swan model, and the SWEM model).

swell propagation by storm surge in the coastal and estuarine zone, the multiple-nested wave models were recommended by Xu et al. (2005), in which the large-scale ocean-scale WAVEWATCH 3 (WW3) model provided the nonstationary two-dimensional (2D) wave spectral boundary condition for the nested SWAN model on coastal and estuarine scales.

In this study, three models were integrated for model simulations (Fig. 4), which included the mesoscale meteorological model WRF [weather research and forecasting model (Skamarock et al. 2008)], the third-generation wave model SWAN (Booij et al. 1999; Zijlema 2010), and the three-dimensional hydrodynamic and sediment transport model SWEM [shallow-water equation model (Qi 2007);

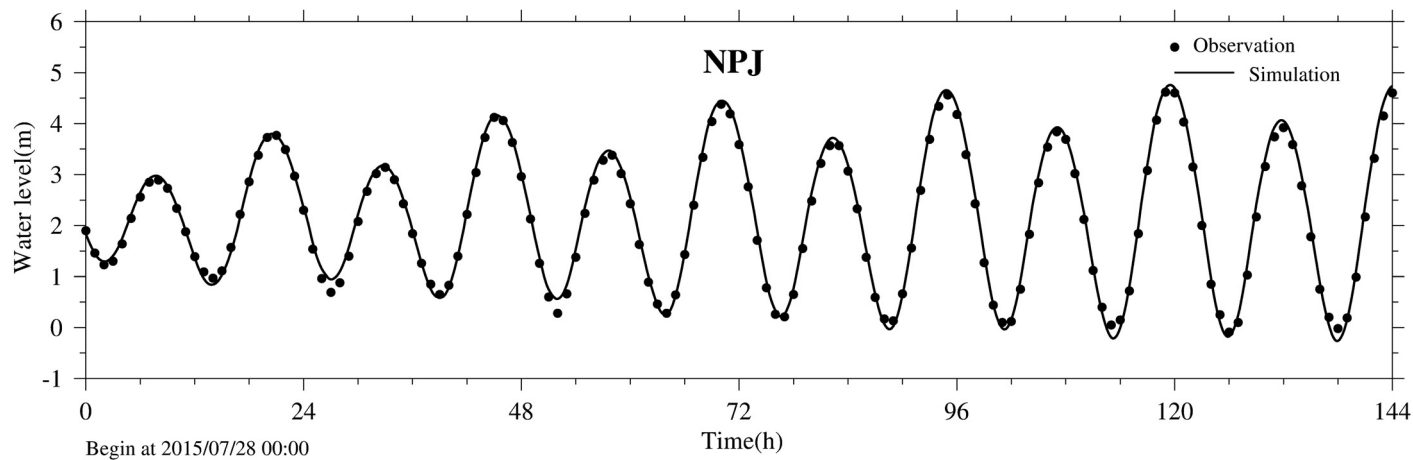


Fig. 6. Comparison of observation and simulation of water level at NPJ station for additional model calibration during the period from July 28 to August 3, 2015.

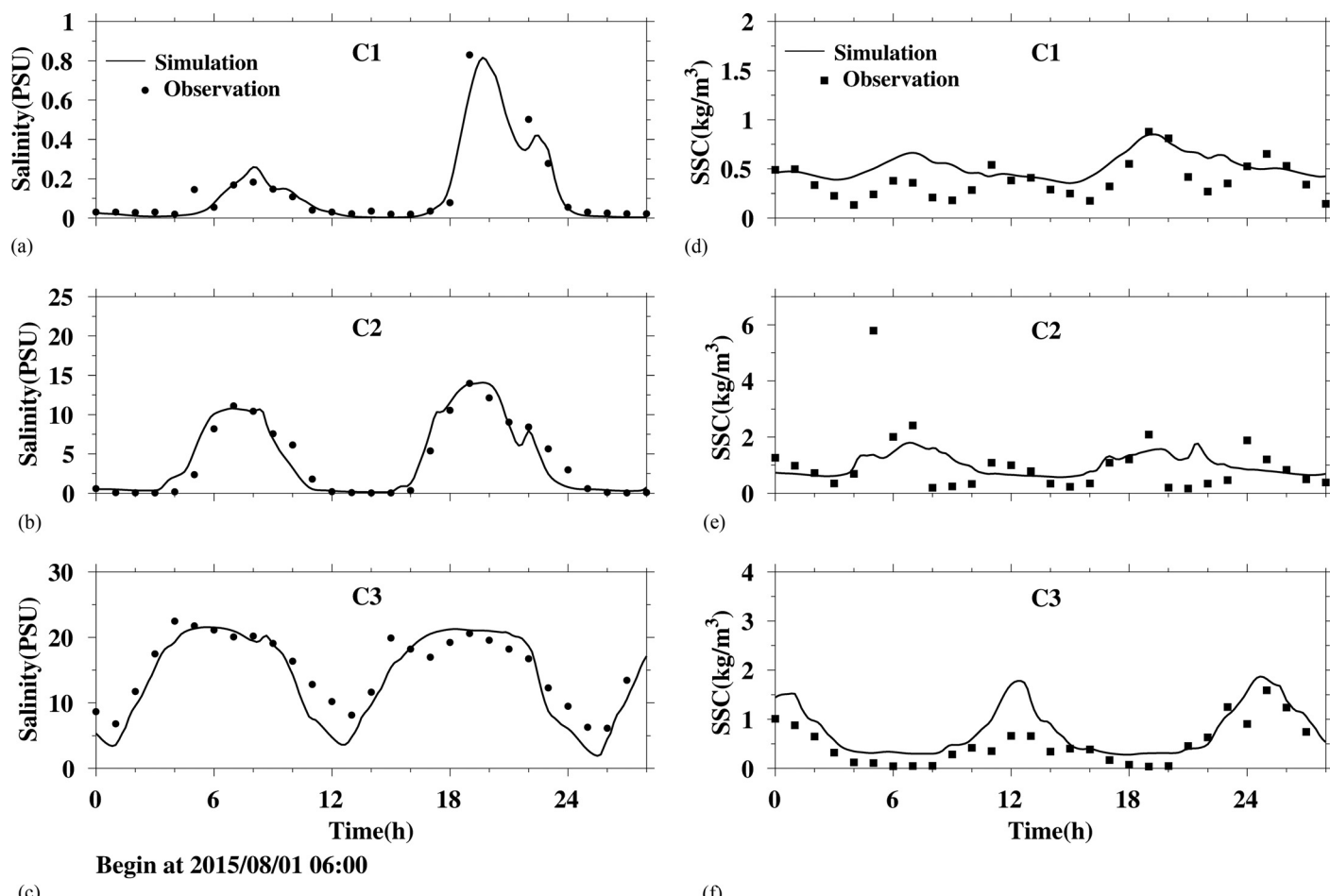


Fig. 7. Comparison of observation and simulation of (a–c) salinity; and (d–f) SSC at C1, C2, and C3 stations for additional model calibration using data from August 2015.

Qi et al. 2010; Shen et al. 2014; Wan et al. 2014). The integrated numerical models were established to simulate the sediment suspension and transport in the north passage of the Changjiang Estuary during the passage of Typhoon Damrey. Following the coupling method proposed by Wang et al. (2006), the framework of the integrated models used for this study is shown in Fig. 4.

Model Setup

In the proposed integrated models, the WRF model provided a high-resolution atmospheric boundary for the SWAN and SWEM models by means of the three-level nesting technique. The three nesting domains (Domains A, B, and C) are shown in Fig. 5. WRF Domain A, with a 50-km resolution, covered the entire East China Sea, Northwest Pacific Ocean, Japan Sea, and South China Sea.

Subdomain B, with a 16-km resolution, had a geographic coverage including the Bohai Sea, Yellow Sea, East China Sea, Taiwan Strait, and the Kuroshio region. The regional domain, with a 5.5-km resolution, covered the Changjiang Estuary, Hangzhou Bay, and adjacent landscape and oceanic regions (Fig. 5, Domain C). The boundary conditions for the WRF model were interpolated from the global real-time data from the National Centers for Environmental Prediction (NCEP) (<https://rda.ucar.edu>). The global real-time data were NCEP Final Operational Global Analysis data (NCEP 2000), which were on 1-degree by 1-degree grids prepared operationally every 6 h. The WRF model was run in parallel under the Linux system from July 1 to August 7, 2012. The model time step set in the WRF model was 100 s.

The third-generation spectral wind-wave model SWAN was used to simulate wave propagation in the Changjiang Estuary. The unstructured flexible mesh was used in the wave model. The model

Table 1. Comparison between observation and simulation for additional SWEM model calibration using data from August 2015

Site	Water level			Salinity			SSC
	NPJ	C1	C2	C3	C1	C2	
Correlation (R)	0.997	0.83	0.91	0.96	0.58	0.62	0.85
RMSE	0.13 m	0.51 psu	2.81 psu	2.77 psu	0.51 kg/m ³	2.81 kg/m ³	2.77 kg/m ³

Note: RMSE = root-mean-square error. The RMSE calculated at the C2 station excluded the one abnormally high SSC, which reached up to 6 kg/m³.

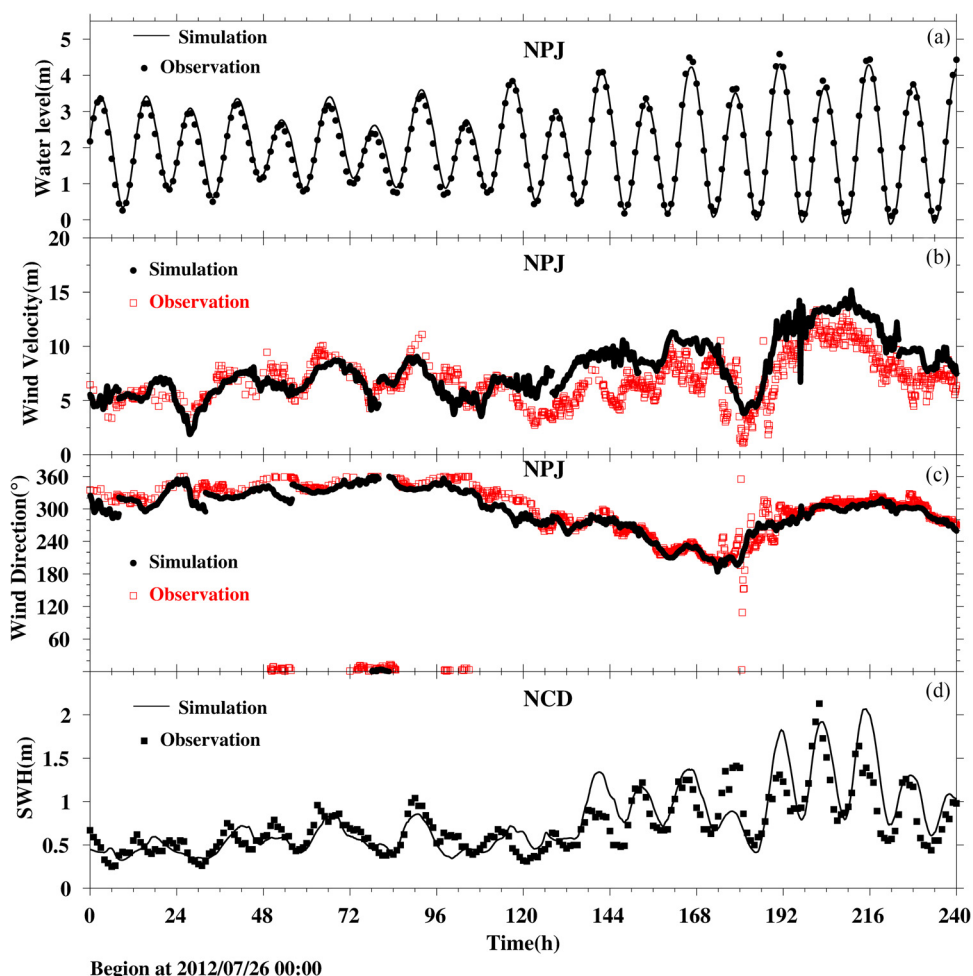


Fig. 8. (Color) Comparison of the simulation with the observation under the model verification during the impact of Typhoon Damrey: (a) water level at NPJ station; (b) wind velocity at NPJ station; (c) wind direction at NPJ station; and (d) SWH at NCD station.

domain covered the Yangtze Estuary, the East Sea, and the West Pacific from approximately 120° east to 130° east and 28° north to 34° north (Fig. 5) for the passage of Typhoon Damrey. With the help of an unstructured grid, the model grid was capable of arbitrary resolution and adequate geographic coverage. Within the Changjiang Estuary, the wave model grid was totally the same as the model grid that was used in the SWEM model (Fig. 5). By this means, the interpolation error during the transferring of two model results was eliminated. In the SWAN model, the surface boundary condition of wind was provided by the WRF model and the field boundary condition of water level and current was provided by the SWEM model. The boundary conditions were inserted into the SWAN model every hour. The model time step set in the SWAN model was 10 min. The SWAN model was run from July 20 to August 7, 2012 under the Windows system.

A three-dimensional, generalized σ -coordinate system, unstructured finite-volume grid, baroclinic estuarine circulation model (SWEM) was built to simulate the complex hydrodynamics and sediment transport in the Changjiang Estuary. More detailed descriptions of the SWEM model structure and calibrations were given by Qi (2007), Qi et al. (2010), Wan et al. (2014), and Shen et al. (2014). In the sediment transport module, both resuspension and deposition

mechanisms depend on the shear stress induced at the sediment–water interface. The Partheniades-Krone formulations (Partheniades 1965) were adopted for the sediment erosion and deposition

$$E = MS(\tau_{cw}, \tau_{cr,e}) \quad (1)$$

$$D = \omega_s C_b S(\tau_{cw}, \tau_{cr,d}) \quad (2)$$

$$S(\tau_{cw}, \tau_{cr,e}) = \begin{cases} \frac{\tau_{cw}}{\tau_{cr,e}} - 1, & \tau_{cw} > \tau_{cr,e} \\ 0, & \tau_{cw} \leq \tau_{cr,e} \end{cases} \quad (3)$$

$$S(\tau_{cw}, \tau_{cr,d}) = \begin{cases} 1 - \frac{\tau_{cw}}{\tau_{cr,d}}, & \tau_{cw} < \tau_{cr,d} \\ 0, & \tau_{cw} \geq \tau_{cr,d} \end{cases} \quad (4)$$

where E = erosion flux ($\text{kg}/\text{m}^2/\text{s}$); M = user-defined erosion rate ($\text{kg}/\text{m}^2/\text{s}$); $S(\tau_{cw}, \tau_{cr,e})$ = erosion step function; D = deposition flux ($\text{kg}/\text{m}^2/\text{s}$); ω_s = settling velocity (m/s); C_b = SSC in the near-bottom computational layer (kg/m^3); $S(\tau_{cw}, \tau_{cr,d})$ = deposition step function; τ_{cw} = bed shear stress due to current and waves (N/m^2); $\tau_{cr,e}$ =

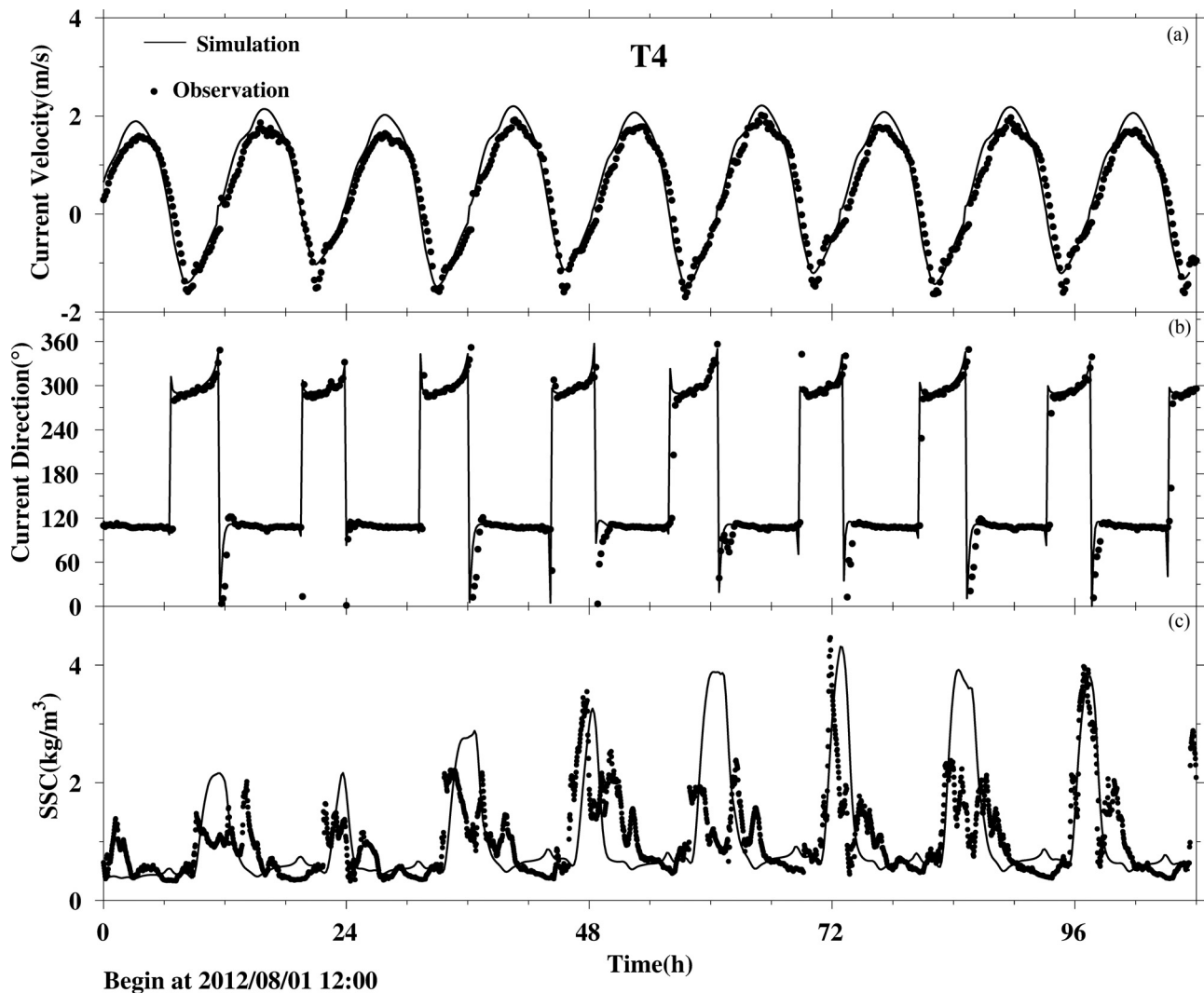


Fig. 9. Comparison of the simulation with the observation at T4 under the model verification during the impact of Typhoon Damrey: (a) vertical averaged tidal velocity; (b) vertical averaged tidal direction; and (c) bottom SSC.

critical erosion shear stress (N/m^2); and $\tau_{cr,d}$ = critical deposition shear stress (N/m^2). The sediment flocculation was considered in the settling velocity based on the experiment results (Wan et al. 2015). Linear-wave theory was used to translate the wave parameters into a near-bed peak orbital velocity and peak orbital amplitude. The bottom shear stress was calculated by the formula proposed by Soulsby et al. (1993) to account for the effects of waves and currents

$$\tau_{cw} = C_d \rho |U|U + \frac{\pi}{8} \rho f_w |U_w|U_w + \frac{B\rho}{\pi} \sqrt{2} (C_d f_w)^{0.5} |U|U_w \quad (5)$$

current wave current-wave interaction

where C_d = bottom friction of current; U = current velocity; U_w = wave orbital velocity; f_w = bottom wave friction; and B = coefficient of wave-current interaction, which can be set to 0.9170, -0.1983, and 0.359 when the wave and current are moved concurrently, perpendicularly, and uncertainly (Soulsby et al. 1993). The first term on the right side of Eq. (5) refers to the current-induced bottom shear stress. The second term on the right side is the wave-induced shear stress, and the third term is the current-wave interaction.

In the SWEM model, the unstructured grid was generated by the Surface-Water Modeling System (SMS) software with a high grid resolution in the area of interest, such as in the north passage. The total number of grid cells was 117,665. The maximum grid resolution was approximately 13 km, and the minimum grid spacing located at the north passage was approximately 70 m. The upstream flux boundary of the model was located at Datong

Station, which was the upper limit of tidal wave, whereas the seaward water level boundary, which was calculated by the harmonic constants, was located eastward at $124^\circ 28'$ east, northward at $34^\circ 16'$ north, and southward at $28^\circ 21'$ north. Vertically, 11 σ -layers were divided uniformly with high resolution both at the water surface and at the bed. The salinity open-boundary condition was retrieved from HYCOM + NCODA Global 1/12° Analysis data (GLBa0.08). The model was run from June 1 to August 7, 2012. The model time step was 30 s, which was run under the Windows system.

Model Calibration and Verification

The SWEM model has previously been calibrated for hydrodynamics, salinity, and sediment transport in the Changjiang Estuary (Qi 2007; Qi et al. 2010; Shen et al. 2014; Wan et al. 2014). In this study, additional model calibration under normal weather conditions during the period from July 28 to August 3, 2015 was conducted to improve model parameters in the sediment transport module. The results of model calibration are shown in Figs. 6 and 7. The locations of the observation stations are shown in Fig. 1. Statistical comparison between model simulations and observations are given in Table 1. For surface water level, the correlation (R) was 0.997 and the root-mean-square error (RMSE) was 0.13 m. For salinity, the correlations were 0.83, 0.91, and 0.96 for C1, C2, and C3. The RMSEs at C1, C2, and C3 were 0.51, 2.81, and 2.77 psu, respectively. For SSC, the model reasonably reflected the variation range of SSC in the north passage. The correlations at C1, C2, and

Table 2. Statistical comparison between simulation and observation during Typhoon Damrey

Name	Wind velocity	Wind direction	SWH	Water level	Current velocity	Current direction	Bottom SSC
Site	NPJ	NPJ	NCD	NPJ	T4	T4	T4
Correlation (R)	0.76	0.96	0.82	0.98	0.97	0.96	0.5
RMSE	2.12 m/s	16.58°	0.22 m	0.19 m	0.28 m/s	27.66°	0.88 kg/m³

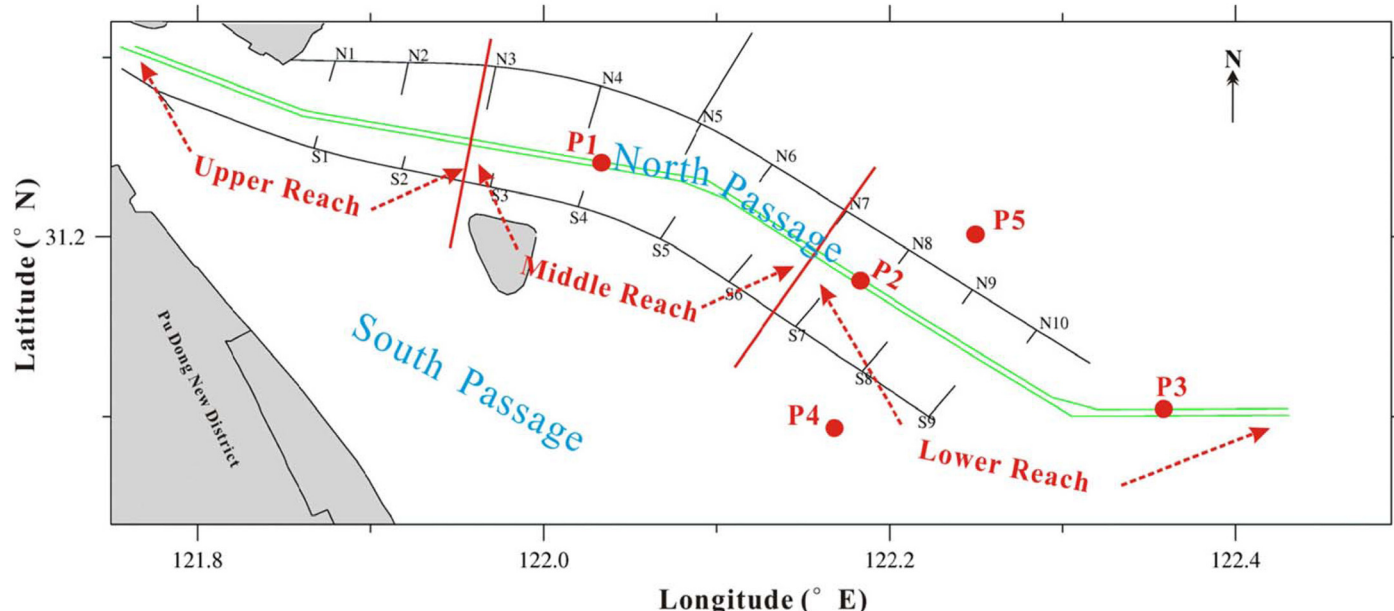


Fig. 10. (Color) Locations of time series of model output (P1–P5). Sites P1–P3, with a depth of 12.5 m, were located along the DNC; P4, with a depth of 5 m, was deployed at the lower reach of the Jiuduansha (JDS) wetland; and P5, with a depth of 5 m, was located at the lower reach of Hengsha Shoal.

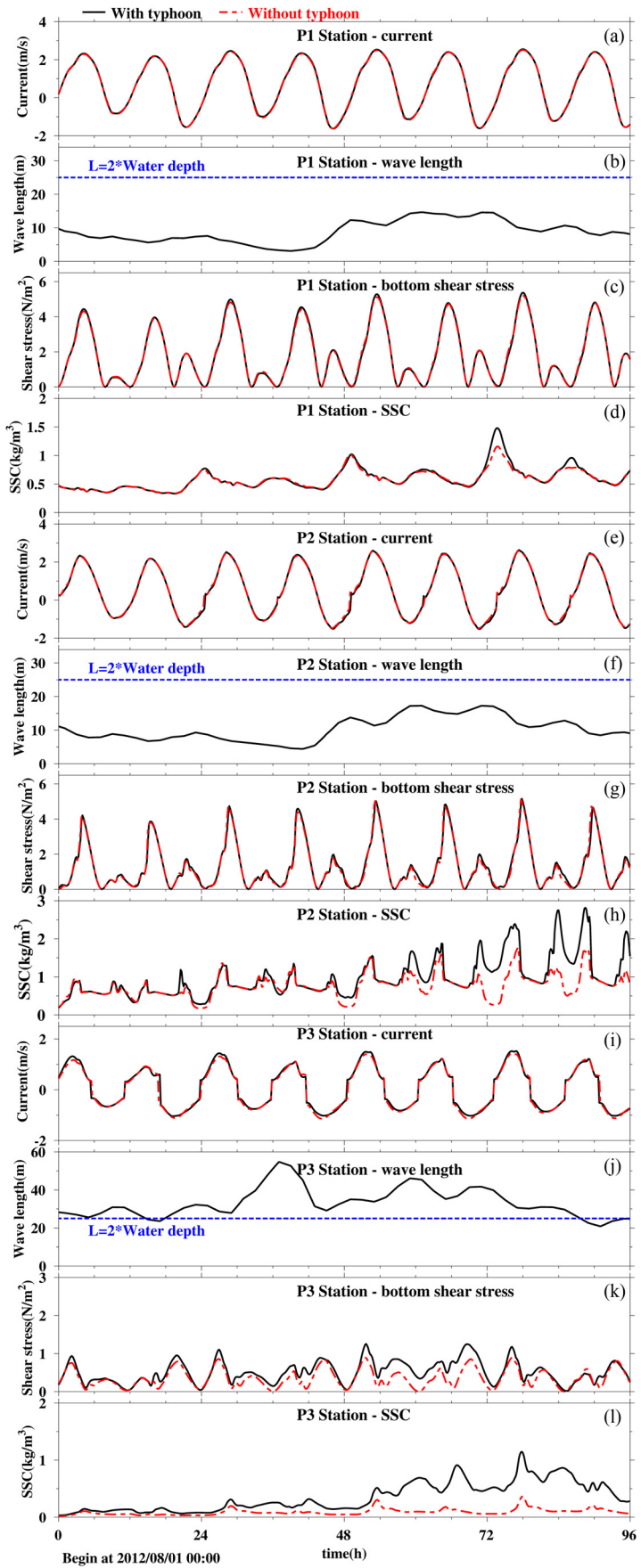


Fig. 11. (Color) Time series variation of the vertical averaged tidal current (a, e, and i), wavelength (b, f, and j), bottom shear stress (c, g, and k), and vertical averaged SSC (d, h, and l) at P1–P3 stations. P1–P3 were deployed along the DNC.

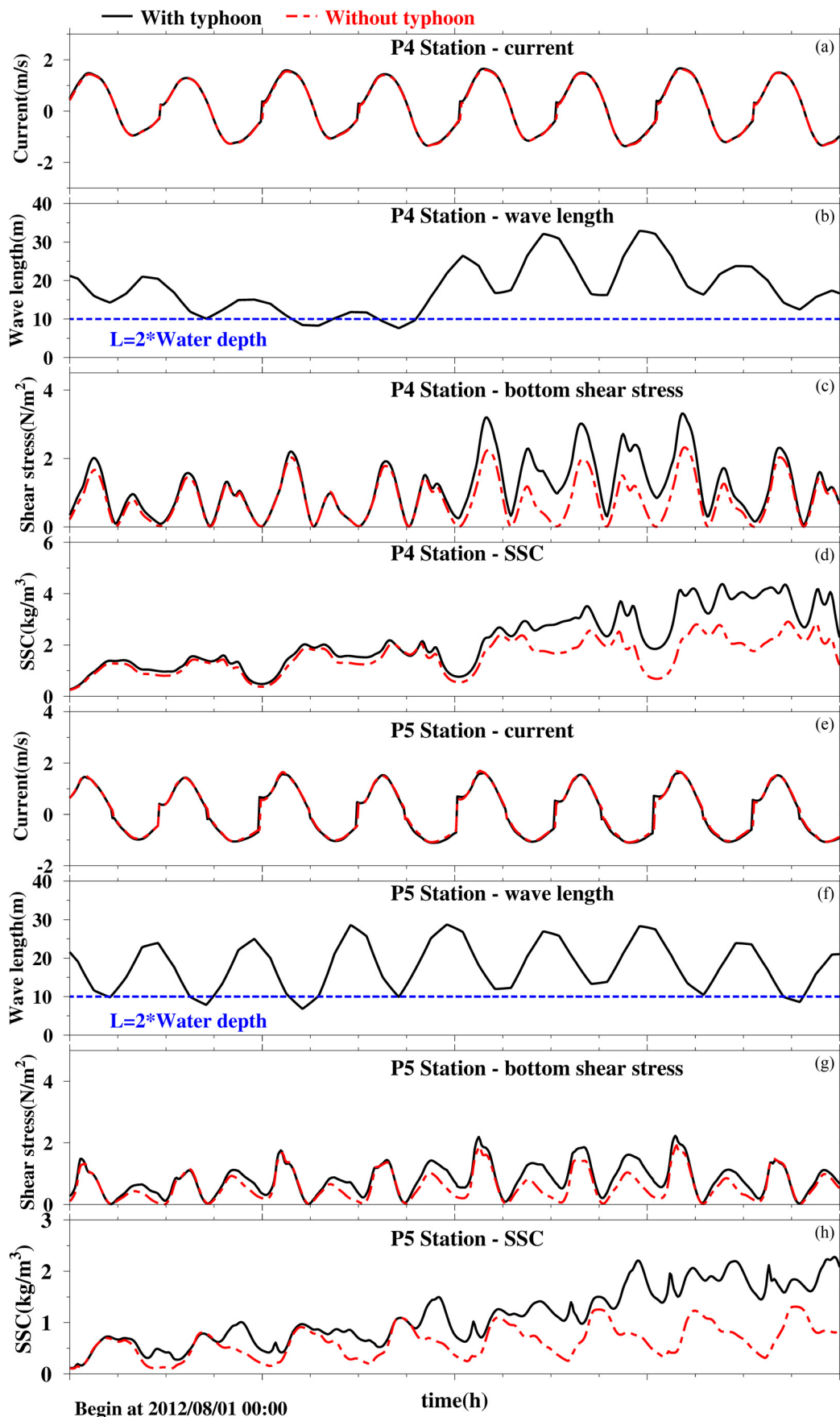


Fig. 12. (Color) Time series variation of the vertical averaged tidal current (a and e), wavelength (b and f), bottom shear stress (c and g), and vertical averaged SSC (d and h) at the P4 and P5 stations. P4 and P5 were deployed at both flank shoals of the north passage.

C3 were 0.58, 0.62, and 0.85, and the RMSEs were 0.51, 2.81, and 2.77 kg/m^3 , respectively.

Based on the model calibration, the parameters in the SWEM model, such as the model bottom roughness and the critical erosion shear stress, were determined. The median grain size of suspended sediment in the Changjiang Estuary was approximately $4\text{--}11 \mu\text{m}$, and the bed load is $8\text{--}120 \mu\text{m}$. Taking the cohesive sediment into account, the model bottom roughness was set to $30 \mu\text{m}$ based on the model calibration. The critical erosion shear stress varied spatially from 0.2 to 0.4 N/m² due to the large area of the model domain. In the estuary, it was difficult to accurately calculate the erosion rate because it depends on the consolidation of bed and sediment composition. The typical value of this parameter was in the range of 10^{-6} to $10^{-3} \text{ kg/m}^2/\text{s}$ (Ge et al. 2015). According to the previous studies (Hu et al. 2009; Kuang et al. 2013; Ge et al. 2015), the erosion rate in the Changjiang Estuary was in the range of 2.5×10^{-6} to $2 \times 10^{-4} \text{ kg/m}^2/\text{s}$, which was set to $4 \times 10^{-5} \text{ kg/m}^2/\text{s}$ in this study.

The parameters in the WRF model were set by default. In the SWAN model, spectral wave computations were performed at logarithmically spaced frequencies over the range of 0.06–1.6 Hz and 36 directional bins with 10 spacing. The third-generation mode for wind input, quadruplet interactions, and white capping was used. Janssen's expression for exponential growth of wave (Janssen 1989, 1991) was used. In this study, the parameters in the SWAN model were set by default except for the bottom friction coefficient of the Joint North Sea Wave Project (JONSWAP) model (Hasselmann 1973) for wave dissipation by bottom friction. This coefficient is equal to $0.038 \text{ m}^2/\text{s}^3$ for swell conditions (Hasselmann 1973) and $0.067 \text{ m}^2/\text{s}^3$ for wind-sea conditions (Bouws and Komen 1983). After numerical tests to examine the sensitivity of this parameter, the best match after comparison with data was found, and the coefficient of the JONSWAP formulation was set to $0.057 \text{ m}^2/\text{s}^3$ in this study.

The previously calibrated hydrodynamic model SWEM, after further enhancement in this study, was used to simulate the hydrodynamics and the sediment transport during the passage of Typhoon Damrey. Time series of water level, winds, SWH, currents, and SSC are presented in Figs. 8 and 9. Observed salinity during the passage of Typhoon Damrey was not available for further model validations. Fig. 8 shows that the simulated water level, wind speed and direction, and SWH were in good agreement with the observations during Typhoon Damrey. This indicates that the

coupled SWAN and WRF models provided suitable boundary conditions for the hydrodynamic model. The comparison of observation and simulation of the tidal current and bottom SSC during the passage of Typhoon Damrey showed a reasonable match between simulations and observations (Fig. 9). As shown in the statistical comparisons (Table 2), wind speed and directions, SWH, water level, and tidal current were well represented by the integrated models. The correlations of wind velocity, SWH, water level, and current velocity were 0.76, 0.82, 0.98, and 0.97, respectively. It should be noted that the modeled bottom SSC was not as good as the predicted current velocity. However, to some extent, the model result was reasonable because the rapid soaring of bottom SSC during the passage of Typhoon Damrey was well reflected in the coupled model, and the modeled amplitude of bottom SSC was in good agreement with the observation. The RMSE of modeled bottom SSC was 0.88 kg/m^3 , which was relatively small when compared to the high SSC during Typhoon Damrey. Therefore, the results of model validation were satisfactory and the established model can be used to investigate sediment suspension and transport in the north passage of the Changjiang Estuary during the passage of Typhoon Damrey.

Modeling Effects of Typhoon Damrey on Sediment Transport in the Navigation Channel

The calibrated and validated models were used to investigate the effects of Typhoon Damrey on sediment resuspension in the estuary and navigation channel. Time series of currents, wavelength, bottom shear stress, and SSC in selected locations in the deepwater channel were used to examine how the typhoon affected current, wave, and wave-current-induced bottom stress. By analyzing if bottom stress mainly caused wave-induced bottom velocity, we can identify if waves were the major cause of change in sediment resuspension at the selected locations. Spatial distributions of currents and sediment concentrations were also used to investigate the sediment transport by estuarine circulations after sediment resuspension during the typhoon. As shown in Eq. (5), bottom shear stresses were affected by both current and wave bottom velocity. Generally, wave bottom velocity is close to zero if the wave is in deep water. Based on linear-wave theory, deep water is defined as water depth larger than 2 times the wavelength. Therefore, wavelength was included in the time series to explain the effects of wave on bottom shear stress.

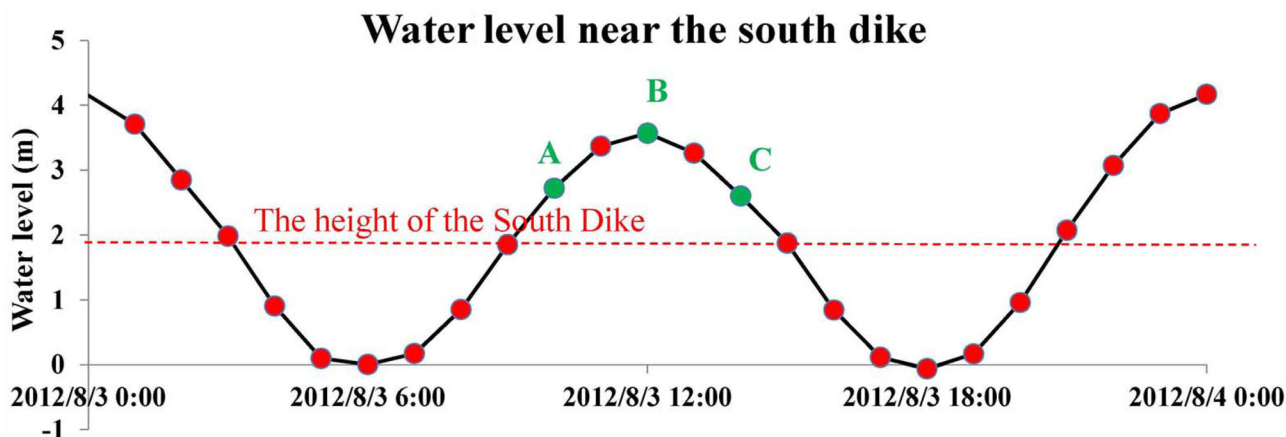


Fig. 13. (Color) Water level near the south dike in the north passage of Changjiang Estuary during the impact of Typhoon Damrey. The green point refers to the three selected time slots at which the water levels at the south flank of the north passage were higher than the height of the south dike.

Time Series Dynamic Analysis of Currents, Wavelength, Bottom Shear Stress, and SSC

To analyze Typhoon Damrey's effects on sediment suspension and transport, the simulation under typhoon conditions and the

simulation without the impact of a typhoon were compared. For the scenario without typhoon, the simulation was conducted without wind forcing and wave. Fig. 10 shows the stations for time series outputs with three stations in the navigation channel and two stations in shallow-water areas outside the channel.

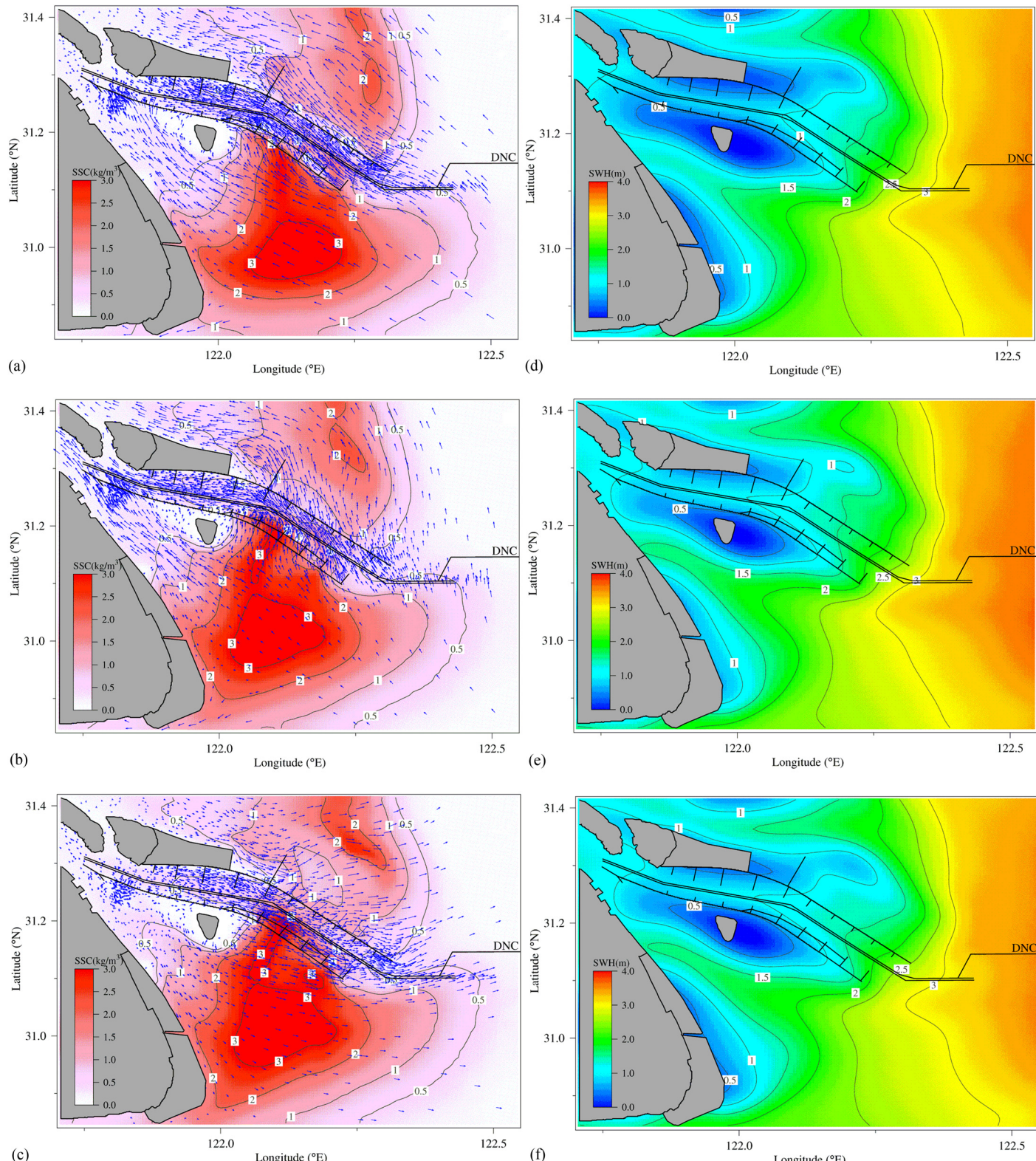


Fig. 14. (Color) Snapshot of the modeled distribution of the tidal current, SSC, and SWH during the passage of Typhoon Damrey corresponding to the selected time slots of (a and d) flood tide; (b and e) high tide; and (c and f) ebb tide displayed in Fig. 13.

Time Series Variation in the DNC

At three stations along the navigation channel, currents were nearly unchanged (Fig. 11) during Typhoon Damrey, indicating that the effect of storm surge can be negligible. The storm wave had little impact on either currents or bottom shear stress at the upper and middle reach of the north passage (P1 and P2, Fig. 11). Based on the linear-wave theory, waves at the P1 and P2 stations were deepwater waves because the wavelength at P1 and P2 was smaller than 2 times the in situ water depth. Because both bottom current and wave velocity were not changed, the bottom shear stresses at P1 and P2 during Typhoon Damrey were not increased. Therefore, the bottom shear stress affected by waves was not increased during the impact of Typhoon Damrey. Therefore, the variations of SSC at the upper and middle reach, as shown at Stations P1 and P2 of the north passage, were not caused by local sediment suspension. At the P3 site, which was at the outlet of the north passage, waves at the P1 and P2 stations were not deepwater waves [Fig. 11(j)]. As a result, the typhoon-induced wave caused some increase of bottom shear stress [Fig. 11(k)] and some increase of SSC [Fig. 11(L)].

Time Series Variation in Shallow-Water Areas outside the Navigation Channel

At two stations (P4 and P5) in the shallow-water areas outside the navigation channel, as shown in Fig. 10, the calculated wavelength was greater than the critical influencing wavelength or 2 times the water depth (Fig. 12), indicating that the waves were not deepwater waves. The storm wave during Typhoon Damrey prominently increased the bottom shear stress at the lower reach of the Jiuduansha (JDS) wetland and the Hengsha shoal. The current was nearly unchanged during the passage of Typhoon Damrey because of the negligible weak storm surge. The propagation of storm wave poses a more prominent influence on local hydrodynamics. The wave-induced increase of bottom shear stress consequently caused the increase of the SSC, which was almost up to 2 times the SSC under the scenario without a typhoon. Comparing the bottom shear stresses between P4 and P5, the shear stress at the south flank shoal at Station P4 was greater than the shear stress at the north flank shoal at P5. The dynamic bottom shear stresses at the shoals (P4 and P5, Fig. 12) were stronger than those at stations at the DNC (Fig. 11). Within a tidal

cycle, the maximum increase of storm-induced bottom shear stress appeared during the flood tide at the JDS wetland (P4) and Hengsha shoal (P5). This is important for the typhoon's effect on sediment suspension and transport. The storm-induced increased bottom shear stress would stir up more sediment at shoals during the flood tide and then transport upstream with the flood current, providing the sediment resource in the north passage.

Spatial Distribution of Current, Significant Wave Height, and SSC

To investigate the spatial distribution of the tidal current, SWH, and SSC, three time slots (A, B, and C) were selected during a tide cycle when the water elevation was above the top elevation of the south dike (Fig. 13). As shown in Fig. 14, the SWH was higher at the south passage than the SWH at the north channel. Due to the protections by the south and north dikes along the navigation channel, the SWH in the channel was the smallest compared with those in the areas outside the channel. At the lower reach, where the SWH reached the highest along the north passage, the SWH was more than 3 m. The distribution of the vertical averaged SSC was totally different among the three outlets in the Changjiang Estuary (the south passage, the north passage, and the north channel). The SSC was highest at the south passage, whereas the SSC at the north channel was lower. At Time Slot A (flood tide), the water level at the south flank of the north passage was higher than the height of the south dike. A high sediment cloud with concentration more than 2 kg/m^3 began to move into the north passage. When the water level was increasing (Fig. 13, Time Slot B), the SWH was enhanced and a higher sediment cloud with concentration greater than 3 kg/m^3 appeared at the lower reach of the JDS wetland south of the navigation channel [Figure 14(b)]. This high sediment cloud was then transported into the navigation channel by the flood current. At Time Slot C, when the flood current was turning into the ebb current [Fig. 14(c)], the high sediment cloud began to move offshore. Therefore, model simulations clearly showed that the increase of SSC in the navigation channel was mainly caused by the sediment transport from the overtopping sediment flux from

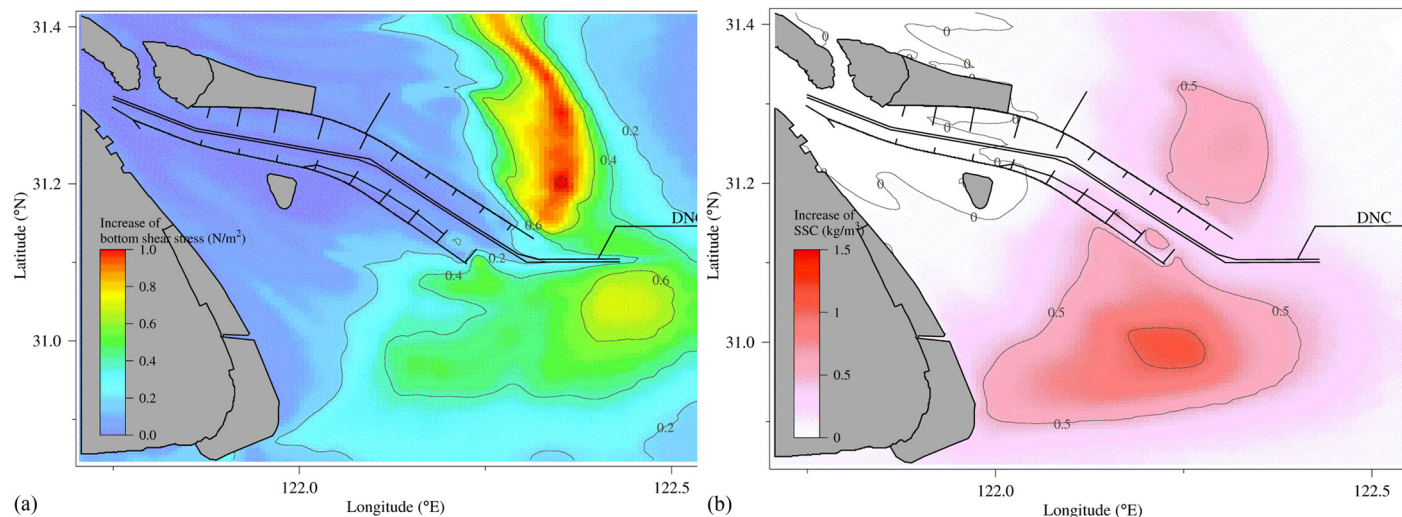


Fig. 15. (Color) Spatial distributions: (a) time-averaged storm-induced increase of bottom shear stress; and (b) vertical averaged SSC, calculated from August 1 to August 5 during the impact of Typhoon Damrey.

shallow-water areas south of the dike during the passage of Typhoon Damrey.

Spatial Distributions of Increased Bottom Shear Stress and SSC during Typhoon Damrey

During the passage of Typhoon Damrey, the storm surge in the Changjiang Estuary was negligible, and the SWH was prominent at the mouth of the Changjiang Estuary. Therefore, the most prominent impact of Typhoon Damrey could have been caused by the wave-induced increase of the bottom shear stress and the SSC. In this study, the wave-induced increase of bottom shear stress was estimated by the wave orbital velocity and the wave-current interaction proposed by Soulsby et al. (1993). To evaluate the impact of Typhoon Damrey on bottom shear stress, spatial distributions of wave-induced increase of bottom shear stress were averaged from August 1 to August 5. Results (Fig. 15)

showed the spatial variations of wave-induced increases of bottom shear stress during the passage of Typhoon Damrey. At the upper and middle reach of the north passage, the increase of bottom shear stress was negligible (with a value less than 0.2 N/m^2 on average). At the lower reach of the north passage, the increase of the bottom shear stress was prominent, ranging from 0.2 to 0.6 N/m^2 . At the lower reach of the DNC, the increase of the bottom shear stress was smaller than the adjacent region due to the limited influence of the wind wave in the deep water. The greatest increase of bottom shear stress was located in the shallow-water area Hengsha shoal north of the navigation channel, which reached up to 1 N/m^2 . In the shallow-water areas south of the navigation channel, the depth the shallow subtidal shoal ranged from 5 to 10 m. Wave-induced increase of bottom stress was approximately 0.4 – 0.6 N/m^2 , which was smaller than the increased magnitude at the Hengsha shoal north of the channel. However, the spatial distribution of the increased SSC was quite different from

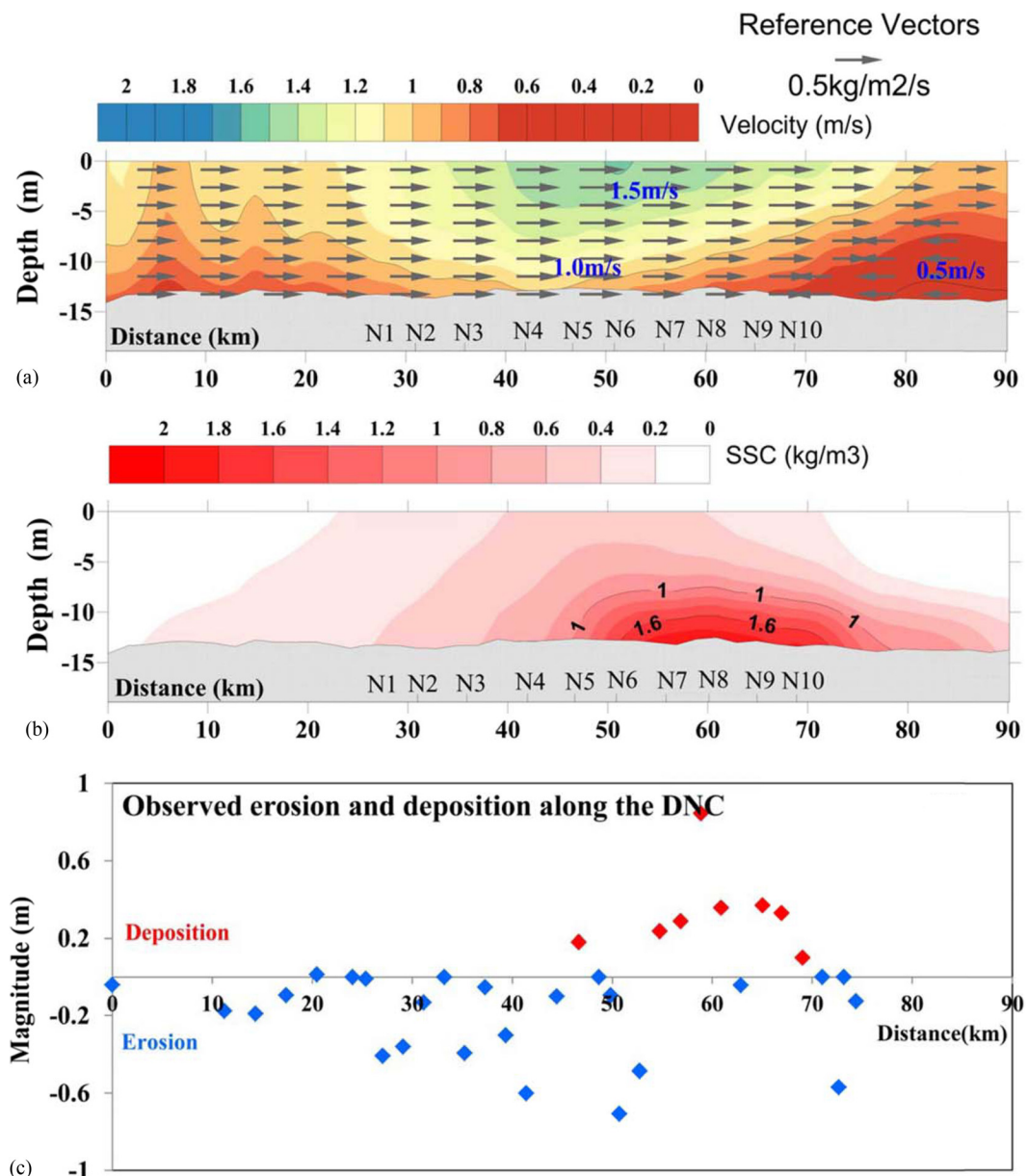


Fig. 16. (Color) Along-channel distributions: (a) residual transport currents averaged from August 1 to August 5; (b) averaged SSC from August 1 to August 5 during Typhoon Damrey; and (c) measured bed erosion and deposition during the passage of Typhoon Damrey.

the increase of the bottom shear stress. A relatively higher increased SSC, with a value greater than 1 kg/m^3 , existed at the outlet of the south passage, whereas at the Hengsha shoal, the increase of the SSC was approximately $0.5\text{--}1 \text{ kg/m}^3$, which was smaller. The phenomenon can be explained by the different sediment grain sizes between the north channel and the south passage. The bed sediment, with a media grain size ranging from 60 to $120 \mu\text{m}$, both at the north channel and the Hengsha shoal, was coarser than the sediment at the north passage and at the south passage, where the media grain size was approximately $20 \mu\text{m}$ (Ge et al. 2015). Thus, sediment at the south passage is easier to suspend than the sediment at both the north channel and the Hengsha shoal.

Discussions on Residual Currents and Sediment Deposition in the Channel

To investigate the erosion and deposition during Typhoon Damrey at the north passage of Changjiang Estuary, two boat-based topographic surveys were conducted before and after Typhoon Damrey. The prestorm measurements were conducted from July 31 to August 1, 2012, and the poststorm measurement was conducted on August 5, 2012. The measured erosion and deposition along the central line of the navigation channel are presented in Fig. 16(c). During the passage of Typhoon Damrey, an intensive erosion

area with a magnitude ranging from 0.2 to 0.8 m appeared at the middle reach of the north passage (approximately 40–50 km). The obvious deposition area with a magnitude ranging from 0.1 to 1.1 m appeared at the lower reach of the north passage (approximately 50–70 km).

To investigate the correlation between sediment deposition and residual currents and SSC in the north passage during the impact of Typhoon Damrey, averaged residual currents and SSC from August 1 to August 5 were used to analyze the net transport of sediment. In the middle reach, the current dynamic was strongest along the north passage [Fig. 16(a)]. The convergence of residual sediment transport is generally recognized as sediment trapping (Traykovski et al. 2004), which could be responsible for the high sedimentation rate (Li et al. 2016). Near the outlet of the north passage near N9–N10 [Fig. 16(a)], an upstream landward residual current existed at the bottom layer, which was against the landward currents [Fig. 16(a)]. Convergence of sediment transport existed in the lower reach of the north passage between N7 and N10 [Fig. 17(b)]. The prominent convergence of sediment in the north passage was formed by the upstream seaward transport of sediment and the downstream lateral transport of sediment, which climbed from the south dike at the middle-lower reach of the north passage. Therefore, a relatively higher sediment cloud existed in the lower reach of the DNC, with a SSC of 1.6 kg/m^3 accumulating at the bottom layer between N7 and N10 along the channel [Fig. 16(b)]. The high SSC zone was consistent in areas with measured sediment deposition (Fig. 16(c)).

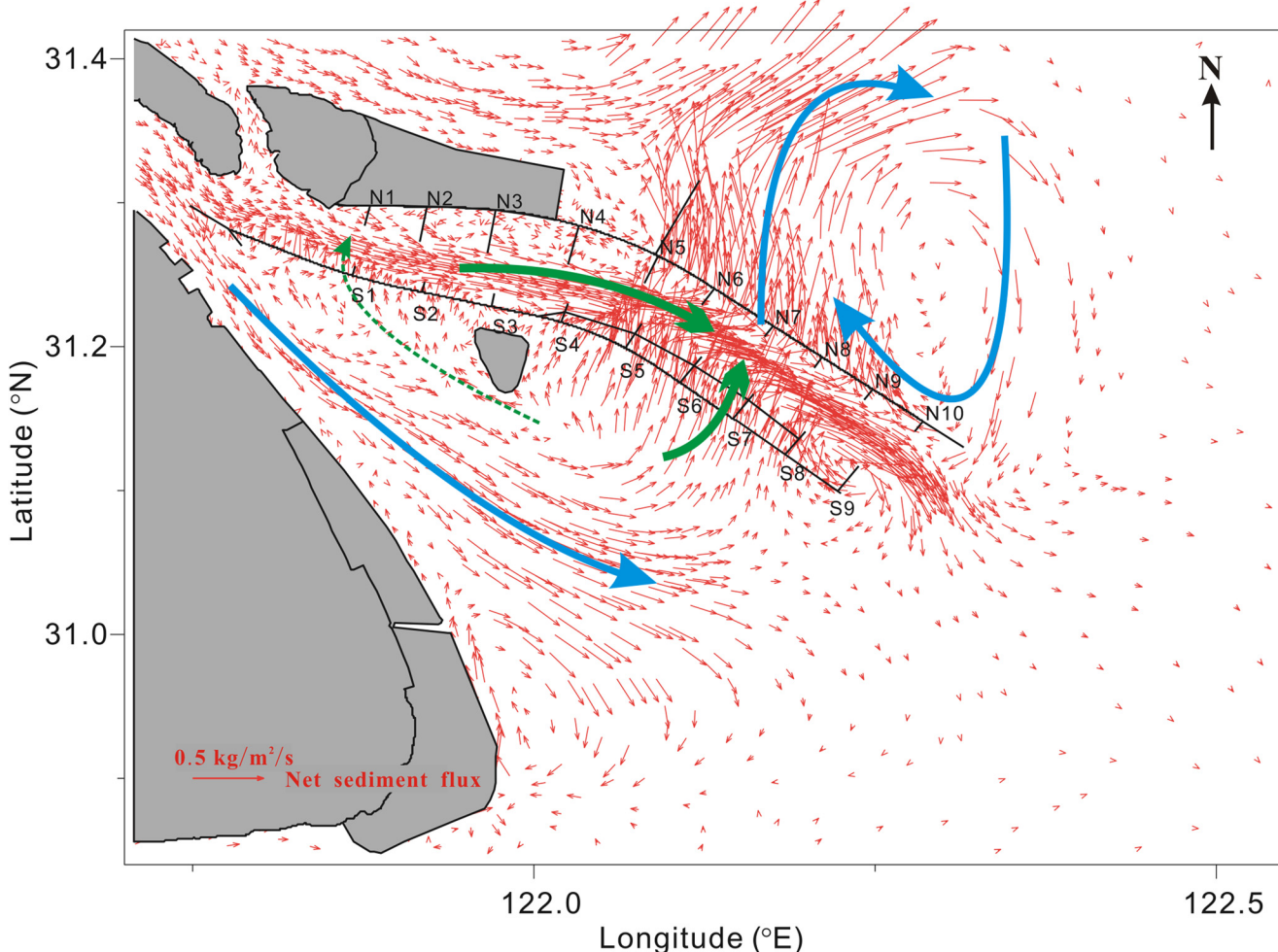


Fig. 17. (Color) Residual transport of sediment calculated from August 1 to August 5 during the passage of Typhoon Damrey.

Conclusion

The effect of Typhoon Damrey on sediment suspension and transport in the north passage of the Changjiang Estuary was investigated by an integrated model study. The previously calibrated hydrodynamic and sediment transport model SWEM was integrated with a storm wind model (WRF) and a wave model (SWAN) to investigate the effect of Typhoon Damrey on the navigation channel in 2012. Typhoon Damrey caused a weak storm surge but strong wave height in the Changjiang Estuary, which provided a good case study for investigating wave effects on wave-current-induced bottom shear stress. The previously calibrated hydrodynamic model (SWEM) was further improved in this study. The integrated models were satisfactorily validated by field observations of waves, currents, and SSC during Typhoon Damrey.

Model simulations of time series of currents, wavelength, and bottom shear stress were used to analyze the causes of the changes in bottom shear stress. Results indicated that currents showed almost no change because of the very weak storm surge during the typhoon. Therefore, the changes of bottom shear stress were mainly induced by the changes of wave conditions during Typhoon Damrey. In the upper and middle channel, bottom shear stresses were not changed because of the deepwater wave conditions (wavelength <2 times water depth). As a result, changes of sediment resuspension in the channel did not occur during the typhoon. In shallow-water areas outside the channel, shallow-water waves caused the increase of bottom shear stress and induced the increase of sediment resuspension.

Model simulations of spatial distributions of currents and sediment concentrations clearly showed that sediment resuspension in the shallow-water area outside the south dike moved into the deepwater channel. This caused the increase of sediment concentration in the channel even though the bottom shear stress did not change under the deepwater wave conditions in the channel. During the flood tide, the high sediment flux overtopped from the south dike into the north passage when the water level was higher than the height of the south dike, which subsequently increased the sediment concentration in the north passage significantly. Model-simulated residual currents and averaged SSC along the channel central line during the typhoon were used to analyze the cause of sediment deposition as observed after the typhoon. The modeled high-turbidity zone in the lower channel reach was consistent with the observed sediment deposition area in the channel. This showed that, although storm surge was negligible during Typhoon Damrey, wave-induced sediment resuspension in the shallow-water area still caused the increase of sediment concentration channel by current-induced sediment flux overtopping into the channel from the south dike, and resulted in sediment deposition near the lower channel reach.

Acknowledgments

This study was sponsored by the Shanghai Municipal Natural Science Fund of China (Grant 14ZR1420700), the National Natural Science Foundation of China (Grant 51279143), and the National Key R&D Program (Grants 2017YFC0405403 and 2016YFC0402107).

References

- Biria, H., M. Neshaei, A. Ghabraei, and M. Mehrdad. 2015. "Investigation of sediment transport pattern and beach morphology in the vicinity of submerged groyne (case study: Dahane Sar Sefidrood)." *Front. Struct. Civ. Eng.* 9 (1): 82–90. <https://doi.org/10.1007/s11709-014-0275-5>.
- Booij, N., R. C. Ris, and L. H. Holthuijsen. 1999. "A third-generation wave model for coastal regions: 1. Model description and validation." *J. Geophys. Res. C Oceans.* 104 (C4): 7649–7666. <https://doi.org/10.1029/98JC02622>.
- Bouws, E., and G. J. Komen. 1983. "On the balance between growth and dissipation in an extreme, depth-limited wind-sea in the southern North Sea." *J. Phys. Oceanogr.* 13 (9): 1653–1658. [https://doi.org/10.1175/1520-0485\(1983\)013<1653:OTBBGA>2.0.CO;2](https://doi.org/10.1175/1520-0485(1983)013<1653:OTBBGA>2.0.CO;2).
- Brown, J. M., R. Bolaños, and J. Wolf. 2013. "The depth-varying response of coastal circulation and water levels to 2D radiation stress when applied in a coupled wave-tide-surge modelling system during an extreme storm." *Coastal Eng.* 82, 102–113. <https://doi.org/10.1016/j.coastaleng.2013.08.009>.
- Cañizares, R., and J. L. Irish. 2008. "Simulation of storm-induced barrier island morphodynamics and flooding." *Coastal Eng.* 55 (12): 1089–1101. <https://doi.org/10.1016/j.coastaleng.2008.04.006>.
- Chen, J., D. Li, B. Chen, F. Hu, H. Zhu, and C. Liu. 1999. "The processes of dynamic sedimentation in the Changjiang Estuary." *J. Sea Res.* 41 (1–2): 129–140. [https://doi.org/10.1016/S1385-1101\(98\)00047-1](https://doi.org/10.1016/S1385-1101(98)00047-1).
- Chen, S. S., W. Zhao, M. A. Donelan, and H. L. Tolman. 2013. "Directional wind-wave coupling in fully coupled atmosphere–wave–ocean models: Results from CBLAST-hurricane." *J. Atmos. Sci.* 70 (10): 3198–3215. <https://doi.org/10.1175/JAS-D-12-0157.1>.
- Dai, H., M. Ye, and A. W. Niedoroda. 2015. "A model for simulating barrier island geomorphologic responses to future storm and sea-level rise impacts." *J. Coastal Res.* 31 (5): 1091–1102. <https://doi.org/10.2112/JCOASTRES-D-14-00094.1>.
- Ding, P. X., H. U. Ke-Lin, Y. Z. Kong, and H. U. De-Bao. 2003. "Numerical simulation of storm-induced erosion/deposition in Yangtze Estuary—A case study of Typhoon Jelawat." *J. Sediment Res.* 6, 18–24.
- Fan, D., Y. Guo, P. Wang, and J. Z. Shi. 2006. "Cross-shore variations in morphodynamic processes of an open-coast mudflat in the Changjiang Delta, China: With an emphasis on storm impacts." *Cont. Shelf Res.* 26 (4): 517–538. <https://doi.org/10.1016/j.csr.2005.12.011>.
- Fettweis, M., F. Francken, D. Van den Eynde, T. Verwaest, J. Janssens, and V. Van Lancker. 2010. "Storm influence on SPM concentrations in a coastal turbidity maximum area with high anthropogenic impact (southern North Sea)." *Cont. Shelf Res.* 30 (13): 1417–1427. <https://doi.org/10.1016/j.csr.2010.05.001>.
- Freeman, A. M., F. Jose, H. H. Roberts, and G. W. Stone. 2015. "Storm induced hydrodynamics and sediment transport in a coastal Louisiana lake." *Estuarine Coastal Shelf Sci.* 161, 65–75. <https://doi.org/10.1016/j.ecss.2015.04.011>.
- Fumin, X., Z. Changkuan, M. Lihua, and T. Jianfeng. 2008. "Effects of storm waves on rapid deposition of sediment in the Yangtze Estuary channel." *Water Sci Eng.* 1 (1): 27–36. [https://doi.org/10.1016/S1674-2370\(15\)30016-8](https://doi.org/10.1016/S1674-2370(15)30016-8).
- Ge, J., F. Shen, W. Guo, C. Chen, and P. Ding. 2015. "Estimation of critical shear stress for erosion in the Changjiang Estuary: A synergy research of observation, GOCE sensing and modeling." *J. Geophys. Res. Oceans.* 120 (12): 8439–8465. <https://doi.org/10.1002/2015JC010992>.
- Goleij, H., A. H. Haghabi, and A. Parsaie. 2017. "An experimental study on plunging depth of density currents." *Front. Struct. Civ. Eng.* 11 (4): 388–395. <https://doi.org/10.1007/s11709-017-0417-7>.
- Gu, J., B. Han, J. Huang, and W. Li. 2010. "Simulation to investigate the essential reasons of typhoon induced siltation in Changjiang River Estuary and the impact to water source area." In *Proc., Int. Conf. on Bioinformatics and Biomedical Engineering*, 1–5. New York: Institute of Electrical and Electronics Engineers.
- Guo, Y., J. Zhang, L. Zhang, and Y. Shen. 2009. "Computational investigation of typhoon-induced storm surge in Hangzhou Bay, China." *Estuarine Coastal Shelf Sci.* 85 (4): 530–536. <https://doi.org/10.1016/j.ecss.2009.09.021>.
- Han, S. L., and K. O. Kim. 2015. "Storm surge and storm waves modelling due to Typhoon Haiyan in November 2013 with improved dynamic meteorological conditions." *Procedia Eng.* 116, 699–706. <https://doi.org/10.1016/j.proeng.2015.08.353>.

- Han, Y., and C. Lu. 2015. "Process research on estuarine turbidity maximum and mouth bar of Yangtze Estuary after the improvement works." *Procedia Eng.* 116, 80–87. <https://doi.org/10.1016/j.proeng.2015.08.267>.
- Hasselmann, K. 1973. "Measurements of wind-wave growth and swell decay during the Joint North Sea Wave Project (JONSWAP)." *Dtsch. hydrogr.z.* 12 (2): 1–95.
- Houser, C., C. Hapke, and S. Hamilton. 2008. "Controls on coastal dune morphology, shoreline erosion and barrier island response to extreme storms." *Geomorphology*. 100 (3–4): 223–240. <https://doi.org/10.1016/j.geomorph.2007.12.007>.
- Hu, K., P. Ding, Z. Wang, and S. Yang. 2009. "A 2D/3D hydrodynamic and sediment transport model for the Yangtze Estuary, China." *J. Mar. Syst.* 77 (1–2): 114–136. <https://doi.org/10.1016/j.jmarsys.2008.11.014>.
- Huang, W. P. 2017. "Modelling the effects of typhoons on morphological changes in the estuary of Beinan, Taiwan." *Cont. Shelf Res.* 135, 1–13. <https://doi.org/10.1016/j.csr.2017.01.011>.
- Janssen, P. A. E. M. 1989. "Wave-induced stress and the drag of air flow over sea waves." *J. Phys. Oceanogr.* 19 (6): 745–772. [https://doi.org/10.1175/1520-0485\(1989\)019<0745:WISATD>2.0.CO;2](https://doi.org/10.1175/1520-0485(1989)019<0745:WISATD>2.0.CO;2).
- Janssen, P. A. E. M. 1991. "Quasi-linear theory of wind-wave generation applied to wave forecasting." *J. Phys. Oceanogr.* 21 (11): 1631–1642. [https://doi.org/10.1175/1520-0485\(1991\)021<1631:QLTOWW>2.0.CO;2](https://doi.org/10.1175/1520-0485(1991)021<1631:QLTOWW>2.0.CO;2).
- Jia, L., Y. Wen, S. Pan, J. T. Liu, and J. He. 2015. "Wave-current interaction in a river and wave dominant estuary: A seasonal contrast." *Appl. Ocean Res.* 52, 151–166. <https://doi.org/10.1016/j.apor.2015.06.004>.
- Jin, K.-R., and Z.-G. Ji. 2005. "Application and validation of three-dimensional model in a shallow lake." *J. Waterway, Port, Coastal, Ocean Eng.* 131 (5): 213–225. [https://doi.org/10.1061/\(ASCE\)0733-950X\(2005\)131:5\(213\)](https://doi.org/10.1061/(ASCE)0733-950X(2005)131:5(213)).
- Kuang, C., X. Liu, J. Gu, Y. Guo, S. Huang, S. Liu, W. Yu, J. Huang, and B. Sun. 2013. "Numerical prediction of medium-term tidal flat evolution in the Yangtze Estuary: Impacts of the Three Gorges project." *Cont. Shelf Res.* 52, 12–26. <https://doi.org/10.1016/j.csr.2012.10.006>.
- Li, J., S. Gao, and Y. Wang. 2010. "Delineating suspended sediment concentration patterns in surface waters of the Changjiang Estuary by remote sensing analysis." *Acta Oceanolog. Sin.* 29 (4): 38–47. <https://doi.org/10.1007/s13131-010-0049-4>.
- Li, J., Q. Liu, and J. Zhou. 2003. "Environmental mechanics research in China." *Adv. Appl. Mech.* 39 (2): 217–306.
- Li, Y., and X. Li. 2016. "Remote sensing observations and numerical studies of a super typhoon-induced suspended sediment concentration variation in the East China Sea." *Ocean Modell.* 104, 187–202. <https://doi.org/10.1016/j.ocemod.2016.06.010>.
- Liu, X., and W. Huang. 2009. "Modeling sediment resuspension and transport induced by storm wind in Apalachicola Bay, USA." *Environ. Modell. Software*. 24 (11): 1302–1313. <https://doi.org/10.1016/j.envsoft.2009.04.006>.
- Li, X., J. Zhu, R. Yuan, C. Qiu, and H. Wu. 2016. "Sediment trapping in the Changjiang Estuary: Observations in the north passage over a spring-neap tidal cycle." *Estuarine Coastal Shelf Sci.* 177, 8–19. <https://doi.org/10.1016/j.ecss.2016.05.004>.
- Lou, S., W. Huang, S. Liu, G. Zhong, and E. Johnson. 2016. "Hurricane impacts on turbidity and sediment in the Rookery Bay National Estuarine Research Reserve, Florida, USA." *Int. J. Sediment Res.* 31 (4): 330–340. <https://doi.org/10.1016/j.ijsrc.2016.06.006>.
- Nakamura, R., O. Takahiro, T. Shibayama, E. Miguel, and H. Takagi. 2015. "Evaluation of storm surge caused by Typhoon Yolanda (2013) and using weather-storm surge-wave-tide model." *Procedia Eng.* 116, 373–380. <https://doi.org/10.1016/j.proeng.2015.08.306>.
- NCEP (National Center for Environmental Prediction). 2000. "NCEP FNL operational model global tropospheric analyses, continuing from July 1999." Research Data Archive at the National Center for Atmospheric Research, Computational and Information Systems Laboratory. Accessed May 28, 2016. <http://rda.ucar.edu/datasets/ds083.2/>.
- Neshaei, M. A. L., and F. Ghanbarpour. 2017. "The effect of sea level rise on beach morphology of Caspian Sea coast." *Front. Struct. Civ. Eng.* 11 (4): 369–379. <https://doi.org/10.1007/s11709-017-0398-6>.
- Palinkas, C. M., J. P. Halka, M. Li, L. P. Sanford, and P. Cheng. 2014. "Sediment deposition from tropical storms in the upper Chesapeake Bay: Field observations and model simulations." *Cont. Shelf Res.* 86, 6–16. <https://doi.org/10.1016/j.csr.2013.09.012>.
- Pan, D., H. Shen, and Z. Mao. 1999. "Formation mechanism and features of the turbidity maximum in the Changjiang River Estuary." *Acta Oceanolog. Sin.* 21 (4): 62–69.
- Pan, Z., and H. Liu. 2015. "Numerical study of typhoon-induced storm surge in the Yangtze Estuary of China using a coupled 3D model." *Procedia Eng.* 116, 849–854. <https://doi.org/10.1016/j.proeng.2015.08.373>.
- Partheniades, E. A. 1965. "Erosion and deposition of cohesive soils." *World J. Biol. Psychiatry* 2 (4): 190–192.
- Qi, D. 2007. *Study and development a numerical computational platform for the Yangtze Estuary waterway and its application*. Report, 144. Shanghai: Estuarine and Coastal Science Research Center.
- Qi, D.-m., G.-f. Ma, F.-f. Gu, and L. Mou. 2010. "An unstructured grid hydrodynamic and sediment transport model for Changjiang Estuary." *J. Hydron., Ser. B.* 22 (5): 1015–1021. [https://doi.org/10.1016/S1001-6058\(10\)60068-6](https://doi.org/10.1016/S1001-6058(10)60068-6).
- Shen, Q., F. Gu, D. Qi, and W. Huang. 2014. "Numerical study of flow and sediment variation affected by sea-level rise in the north passage of the Yangtze Estuary." *J. Coastal Res.* 68 (Fall): 80–88. <https://doi.org/10.2112/SI68-011.1>.
- Shen, H., S. He, D. Pan, and J. Li. 1992. "A study of turbidity maximum in the Changjiang estuary." *Acta Geographica Sin.* (5): 472–479.
- Skamarock, W. C., J. B. Klemp, J. Dudhia, D. O. Gill, D. M. Baker, M. G. Duda, X. Y. Huang, W. Wang, and J. G. Powers. 2008. *A description of the advanced research WRF version 3*. NCAR technical note, 125. Boulder, CO: Powers Mesoscale and Microscale Meteorology Division National Center for Atmospheric Research.
- Soulsby, R. L., L. Hamm, G. Klopman, D. Myrhaug, R. R. Simons, and G. P. Thomas. 1993. "Wave-current interaction within and outside the bottom boundary layer." *Coastal Eng.* 21 (1–3): 41–69. [https://doi.org/10.1016/0378-3839\(93\)90045-A](https://doi.org/10.1016/0378-3839(93)90045-A).
- State Oceanic Administration. 2014. "China Marine Hazards Communiqué." http://www.soa.gov.cn/zwgk/hygb/zghyzhgb/2014nzghyzhgb/201503/t20150318_36389.html.
- Stockdon, H. F., A. H. Sallenger, R. A. Holman, and P. A. Howd. 2007. "A simple model for the spatially-variable coastal response to hurricanes." *Mar. Geol.* 238 (1–4): 1–20. <https://doi.org/10.1016/j.margeo.2006.11.004>.
- Stone, G. W., and D. A. Pepper. 1997. "Overview and significance of hurricanes on the Louisiana coast, U.S.A." *J. Coastal Res.* 13 (3): 656–669.
- Traykovski, P., R. Geyer, and C. Sommerfield. 2004. "Rapid sediment deposition and fine-scale strata formation in the Hudson estuary." *J. Geophys. Res. Earth Surf.* 109 (F2): 239–261. <https://doi.org/10.1029/2003JF000096>.
- Wang, C.-h., W.-h. Wai, Onyx, Y.-s. Li, and Y. Chen. 2006. "Modelling of the wave-current interaction in the Pearl River Estuary." *J. Hydron., Ser. B.* 18 (3): 159–165. [https://doi.org/10.1016/S1001-6058\(06\)60047-4](https://doi.org/10.1016/S1001-6058(06)60047-4).
- Wan, Y., D. Roelvink, W. Li, D. Qi, and F. Gu. 2014. "Observation and modeling of the storm-induced fluid mud dynamics in a muddy-estuarine navigational channel." *Geomorphology*. 217, 23–36. <https://doi.org/10.1016/j.geomorph.2014.03.050>.
- Wan, Y., H. Wu, D. Roelvink, and F. Gu. 2015. "Experimental study on fall velocity of fine sediment in the Yangtze Estuary, China." *Ocean Eng.* 103, 180–187. <https://doi.org/10.1016/j.oceaneng.2015.04.076>.
- Xie, W., Q. He, K. Zhang, L. Guo, X. Wang, J. Shen, and Z. Cui. 2017. "Application of terrestrial laser scanner on tidal flat morphology at a typhoon event timescale." *Geomorphology*. 292, 47–58. <https://doi.org/10.1016/j.geomorph.2017.04.034>.
- Xu, F. M., W. Perrie, J. L. Zhang, Z. Y. Song, and B. Toulany. 2005. "Simulation of typhoon-driven waves in the Yangtze Estuary with multiple-nested wave models." *China Ocean Eng.* 19 (4): 613–624.
- Yan, H., Z. Dai, L. I. Jiufa, J. Zhao, X. Zhang, and J. Zhao. 2011. "Distributions of sediments of the tidal flats in response to dynamic actions, Yangtze (Changjiang)Estuary." *J. Geog. Sci.* 21 (4): 719–732. <https://doi.org/10.1007/s11442-011-0875-0>.

- Yang, S. L., P. Li, A. Gao, J. Zhang, W. X. Zhang, and M. Li. 2007. "Cyclical variability of suspended sediment concentration over a low-energy tidal flat in Jiaozhou Bay, China: Effect of shoaling on wave impact." *Geo-Mar. Lett.* 27 (5): 345–353. <https://doi.org/10.1007/s00367-007-0058-2>.
- Yang, Z., S. Taraphdar, T. Wang, and L. R. Leung. 2016. "Uncertainty and feasibility of dynamical downscaling for modeling tropical cyclones for storm surge simulation." *Nat. Haz.* 84 (2): 1161–1184. <https://doi.org/10.1007/s11069-016-2482-y>.
- Yang, Z., T. Wang, L.-Y. R. Leung, K. A. Hibbard, A. C. Janetos, I. P. Kraucunas, J. S. Rice, B. Preston, and T. Wilbanks. 2014. "A modeling study of coastal inundation induced by storm surge, sea level rise and subsidence in the Gulf of Mexico." *Nat. Haz.* 71 (3): 1771–1794. <https://doi.org/10.1007/s11069-013-0974-6>.
- Yin, K., S. Xu, and W. Huang. 2016. "Modeling sediment concentration and transport induced by storm surge in Hengmen Eastern Access Channel." *Nat. Haz.* 82 (1): 617–642. <https://doi.org/10.1007/s11069-016-2200-9>.
- Zhao, Q. 2007. "SWAN/ECOMSED-based three-dimensional numerical model for fine sediment transport in storm event in Huanghua Port." *J. Sediment Res.* (4): 17–26.
- Zhao, D., J. Liu, and H. Wu. 2012. "Preliminary analysis of typhoon-induced sudden sedimentation in navigation channel in Yangtze Estuary over last decade." *J. Sediment Res.* 2, 009.
- Zhou, J. F., and J. C. Li. 2005. "Modeling storm-induced current circulation and sediment transport in a schematic harbor." *J. Waterway, Port, Coastal, Ocean Eng.* 131 (1): 25–32. [https://doi.org/10.1061/\(ASCE\)0733-950X\(2005\)131:1\(25\)](https://doi.org/10.1061/(ASCE)0733-950X(2005)131:1(25)).
- Zijlema, M. 2010. "Computation of wind-wave spectra in coastal waters with SWAN on unstructured grids." *Coastal Eng.* 57 (3): 267–277. <https://doi.org/10.1016/j.coastaleng.2009.10.011>.